05

Physical principles of development of magneto-levitation systems based on the second generation high temperature superconducting composites (Review)

© I.A. Rudnev, I.V. Anischenko

National Research Nuclear University „MEPhI“,
115409 Moscow, Russia
e-mail: iarudnev@mephi.ru

Received May 27, 2021
Revised July 8, 2021
Accepted July 13, 2021

An overview of experimental and theoretical studies of the characteristics of maglev systems using high-temperature superconductors (HTSC) is presented. Materials used in maglev technologies, namely bulk superconductors and HTSC tape composites, are considered. The main experimental data obtained on both bulk and tape superconductors assembled in stacks of various configurations are demonstrated. The factors influencing the magneto-force characteristics are analyzed: geometric parameters, the influence of external alternating magnetic fields, temperatures, relaxation phenomena. A significant part of the review is devoted to the description of various methods for calculating maglev systems, including those based on stacks of HTSC composites. The features of thermal processes in maglev systems with cryocooler and nitrogen cooling are considered. General recommendations for the creation of optimal maglev systems based on tape HTSC composites are given.

Keywords: magnetic levitation, high-temperature superconductors, strip composites, levitation force, lateral force, methods for calculating magnetic force characteristics.

DOI: 10.21883/TP.2022.15.55257.101-21

Introduction

Magnetic levitation, i.e. stable hovering of one magnetic object above another, at first sight seems to be quite an unusual phenomenon contradicting to common experience. In fact, when trying to approach two magnets with differently directed magnetic-moment vectors to each other they are pushing off of each other quite strongly. Such a pushing force can exceed the gravity force significantly and, the logic goes, we could find a position, in which the gravity force is equal to the pushing one, and it is the position when one magnet will hover above another, demonstrating the levitation phenomenon. But, finding the position is impossible due to instability of a dipole pair system. This fact is directly arising from the classical Earnshaw theorem [1], according to which a stationary object consisting of a set of masses, charges and magnets cannot stably hover in a space under effect of any fixed combination of electrical, magnetic and gravity forces (see also [2]). It is because of the total energy of equilibrium state in external field, that in general case is made up by magnetic, electrostatic and gravitational interaction, must be the minimum one. It is impossible, because potentials of such interactions satisfy the Laplace equations, whose solutions have no minima, i.e. there are no stable positions for levitation in such systems. However, the Earnshaw theorem is applicable to a classical stationary case only. Second-kind superconductors, being ideal diamagnets in the Meissner state and having complex magnetic properties caused by penetration and pinning of Abrikosov vortices, by virtue of their nature refer to quantum objects, therefore, do not satisfy the Earnshaw theorem, as notes Noble Prize Winner A. Heym in his articles [3–5]. It is because of that the levitation of the second-kind superconductors in magnetic field is possible and it is practically observed, namely the stable position of a magnet relative to a superconductor. Superconductor repulsion from the magnet caused by the interaction of currents induced in the superconductor and permanent magnet is possible both for the first-kind superconductors and for the second-kind superconductors in the Meissner state. But the mutual position of the magnet and superconductor in these cases appears to be instable, and the pinning of magnetic flux quantum and Abrikosov vortices in a mixed state (in case of excess by magnetic field of the value of the first critical field for the superconductor) leads to the appearance of stable configurations.

Basically, any diamagnetic objects having negative magnetic susceptibility, even quite low one, can levitate, since diamagnetism is caused by quantum motion of electron by orbital, and not by classical stationary charges. Thus, the works [3–5] describe the possibility of levitation for virtually any objects having weak diamagnetic properties, even for living organisms.

Despite that stable magnetic levitation can be observed for superconductors with any critical temperature T_c, high-temperature superconductors (HTS) with the T_c higher than the liquid nitrogen boiling point are the most appropriate from a practical perspective. This refrigerant is cheap

enough versus other cryogenic liquids and has a high value of the heat of evaporation, which allows using it for cooling superconductors in levitation devices without considerable heat insulation of them. An alternative for HTS cooling down to 77 K and lower, even to the range of helium temperatures, is the use of cryocooler equipment.

This review is devoted to discussion of main properties of magnetic levitation with the use of high-temperature superconductors. It deals with the materials used in magnetic levitation technologies: three-dimensional superconductors, belt HTS-composites, and permanent magnets. We present main experimental data obtained both for three-dimensional and belt superconductors assembled into stacks in various configurations. We will show factors affecting magnetic-force characteristics: geometrical parameters, influence of external variable magnetic fields, temperature, relaxation of levitation force. Major part of the review is devoted to description of different methods of calculation of magnetic levitation systems, including based on the stacks of HTS-composites. Finally, we will show that belt HTS-composites are an essential alternative for three-dimensional HTS that are customarily used for these purposes. Last section presents several examples of magnetic levitation devices.

1. Materials used in superconducting magnetic levitation technologies

1.1. Three-dimensional HTS-materials

The majority of three-dimensional HTS is made of copper-oxide superconductors $REBa_2Cu3O_{7-x}$ (REBCO), where RE refers to a rare earth element [6]. Also, in some cases other superconductors are used, e.g. magnesium diboride MgB_2 or iron-based pnictides [7–10]. The disadvantage of the last two materials is their relatively low critical temperature versus that of REBCO, and the advantage is high values of the irreversibility field characterizing magnetic field ranges of possible application of superconductors.

One of the common examples of REBCO is $YBa_2Cu_3O_{7-x}$ (YBCO or Y123). Yttrium can be replaced with other rare earth elements, e.g. gadolinium. Three-dimensional REBCOs are manufactured, as a rule, by using the melting technologies [11]. Pressed mixed powders, depending on the finished composition required, are placed into a furnace together with a small seed single crystal and undergo heat treatment. In order to increase the quality and rate of manufacture one can place several seeds [15]. As a result, three-dimensional HTS can be quite heterogeneous at the boundaries of the growth sectors (crystallites) [13]. In addition, the products made of HTS represent brittle ceramics, which can be cracking under the effect of stresses of different nature, in particular, during magnetization, this is why an additional mechanical reinforcement thereof is necessary (bandaging) [14].

Usually, three-dimensional superconductors are manufactured as cylinders or discs, though for certain applications three-dimensional materials can be manufactured as rings [15]. At this moment the critical current density J_c of massive HTS falls within the range from 10^8 to 10^9 A/m^2 at 77 K in the absence of external magnetic field. It should be noted that assessment of the value of the critical current density for three-dimensional HTS is a challenging task versus that for belt materials. To perform direct transport measurements it is required to cut rectangular bars that could result in mechanical cracks and, as a consequence, errors of determination of J_c. Other method, which is applied more frequently refers to mapping of captured magnetic flux after application and release of the magnetic field (permanent or pulsed) with further calculation of the critical current density by means of the inversion operation [16,17].

Various methods are used for the synthesis of three-dimensional HTS, whose main goal is to obtain high-density materials with high values of the critical current density. It is achieved by texturing the materials and improving the orientation of grains, improving the conductivity of grain boundaries (absence of weak links between grains) and creation of the centers of pinning of magnetic flux. Main methods of synthesis of materials with a high texturing degree include the following [18,19]:

— slow cooling down in homogeneous temperature field (with zero temperature gradient);

— slow cooling down in gradient temperature field without movement of the sample (Bridgman method);

— gradient crystallization with hot zone movement (Zone-Melt (MZ)) — zone melt method;

— seeded directional solidification (Seeded-Directional-Solidification (SDS));

— top seeded melt growth (Top-Seeded-Melt-Growth (TSMG));

— texturing in the magnetic field, as well as other methods, whose description can be found in the literature [18–30].

An overview of the three-dimensional HTS synthesis methods is given in the recent monograph [31].

1.2. Belt HTS-composites

1.2.1. the first and the second generation HTS-belts

The 1G HTS-belts (1G means the„first generation“) use superconductors $(Bi,Pb)_2Sr_2Ca_2Cu_3O_x$ (BSCCO or Bi2223) or $(Bi,Pb)_2Sr_2CaCu_2O_x$ (Bi2212) (Fig. 1). These two copper-oxide superconductors belong to the same family of bismuth HTS, contain the same elements, but have

Figure 1. Image of cross-section of the first generation HTS-belt (from [32]).

different critical temperature (110 and 84 K, accordingly) due to differences in stoichiometric composition. The main method of the 1G belt manufacture was named the „powder in a tube“. The process includes 3 stages:

1) filling of a metallic HTS tube (as a rule made of silver) with a precursor powder;

2) crimping and rolling of the filled tube;

3) multiple „annealing−rolling“cycles.

A monofilament or polyfilament belt is formed in the process of thermal, mechanical and chemical treatment, which has distinctive cross-section of 4×0.3 mm and the length exceeding 1000 m. As for today, polyfilament belts from the Japanese Corporation Sumitomo Electric Industries have the best characteristics: on the length of 1500−2000 m the critical current is 170−200 A, and on the short samples it exceeds the values of 250 A [32].

However, the technology „powder in a tube“ has a series of disadvantages:

1) the need for the deformation of HTS material in the process of the belt rolling in order to produce a high texturing degree (hence, there is further many-time annealing);

2) a high specific cost, one of the main reasons for which is expensive silver matrix (the filling coefficient for the HTS-material does not exceed 20%!)

3) at the liquid nitrogen boiling point the current-carrying capability of the produced conductors of a bismuth system falls drastically at the increase of external magnetic field, and is virtually absent in the magnetic fields ~ 1 T.

While the first two disadvantages are of a technological origin, i.e. these can be optimized, the last one is caused by the manifestation of intrinsic physical properties of the Bi-based HTS, and relates to a high anisotropy degree of such materials.

Characteristics of different materials in magnetic field are demonstrated on the phase H−T-diagram (Fig. 2). If the H−T-diagram is considered in terms of the second critical field−temperature, the materials demonstrate superconducting properties below the line on the H−T-diagram, and not demonstrate above it. However, from a practical perspective it is more important to consider the H−T-diagram in terms of the field of irreversibility−temperature. In this case the curve H−T determines the range of existence of a non-zero critical current. In case of low temperatures near to the liquid helium boiling point, both the low-temperature, and, even more the high-temperature superconducting materials remain in the superconducting state up to the several dozens Tesla fields. At $T = 77$ K the situation is radically different. Bi-based HTS lose superconducting properties (more specifically, the value of critical current becomes zero) in the field of about one Tesla. The Y123 HTS at the same temperature is capable to preserve superconductivity in the fields of up to 5−8 T, while critical current in the fields exceeding 3 T becomes insufficient for practical applications. It is the REBCO materials that have become the base for the 2G HTS-conductors (2G — second generation).

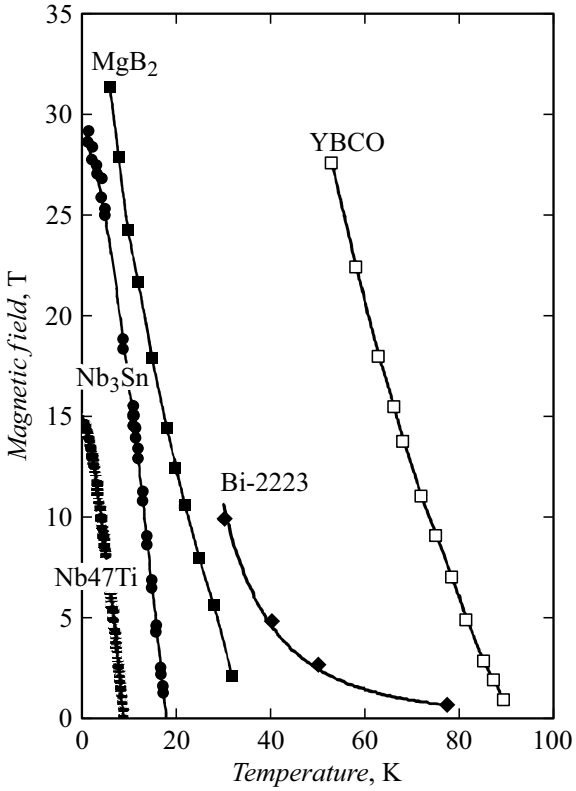

Figure 2. H−T-diagram of different superconducting materials (adapted from [33]).

1.2.2. 2G HTS belts: architecture of composites and manufacturing technologies

The 2G HTS-conductors radically differ from the 1G conductors. It is not only because of the use of different superconducting materials. Simple replacement in the „powder in a tube“ technology of Bi2223 superconductors with Y123 ones failed, because in polycrystalline state $YBa_2Cu_3O_{7-x}$ demonstrate very low critical current density due to a high number of weak links. Main difference between the 1G- and 2G-conductors refers to the application of different process approaches. As already noted above, while the 1G „powder in a tube“ technology is more like a metallurgical process, the 2G conductors are manufactured only by using film technologies. The 1G- and the 2G conductors have different internal structure, accordingly. Fig. 3 shows schemes of cross-sections of the 1G and 2G belts. As we can see, 1G conductors refer to a series of HTS-filaments in a silver matrix. 2G-conductors are an aggregate of thin layers of various materials applied onto a metallic substrate (Fig. 4). A belt made of nickel-based alloy, in particular, Hastelloy is used as a substrate. Several intermediate „buffer“ layers are required to prevent chemical interaction of HTS and a substrate, and the creation of a necessary basic texture. Superficial metallic protective layer prevents HTS from interaction with water and carbon dioxide evaporated from the air; it is a protection against

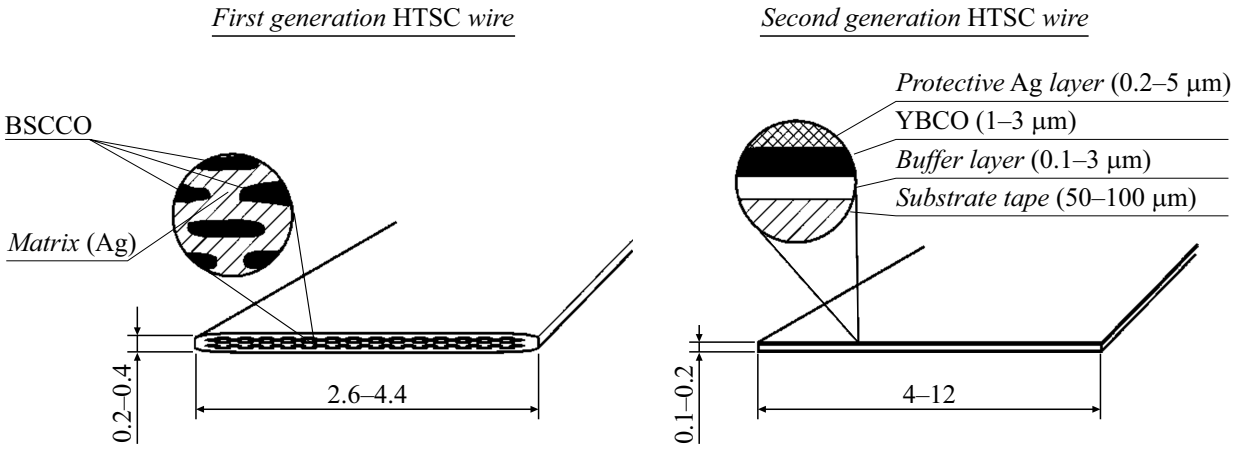

Figure 3. Schematic cross-section of HTS-belts based on BSCCO and YBCO. Typical sizes of belts are provided. Today, BSCCO belts with the width of 4 mm and YBCO belts with the width of 4 and 12 mm are the most common ones.

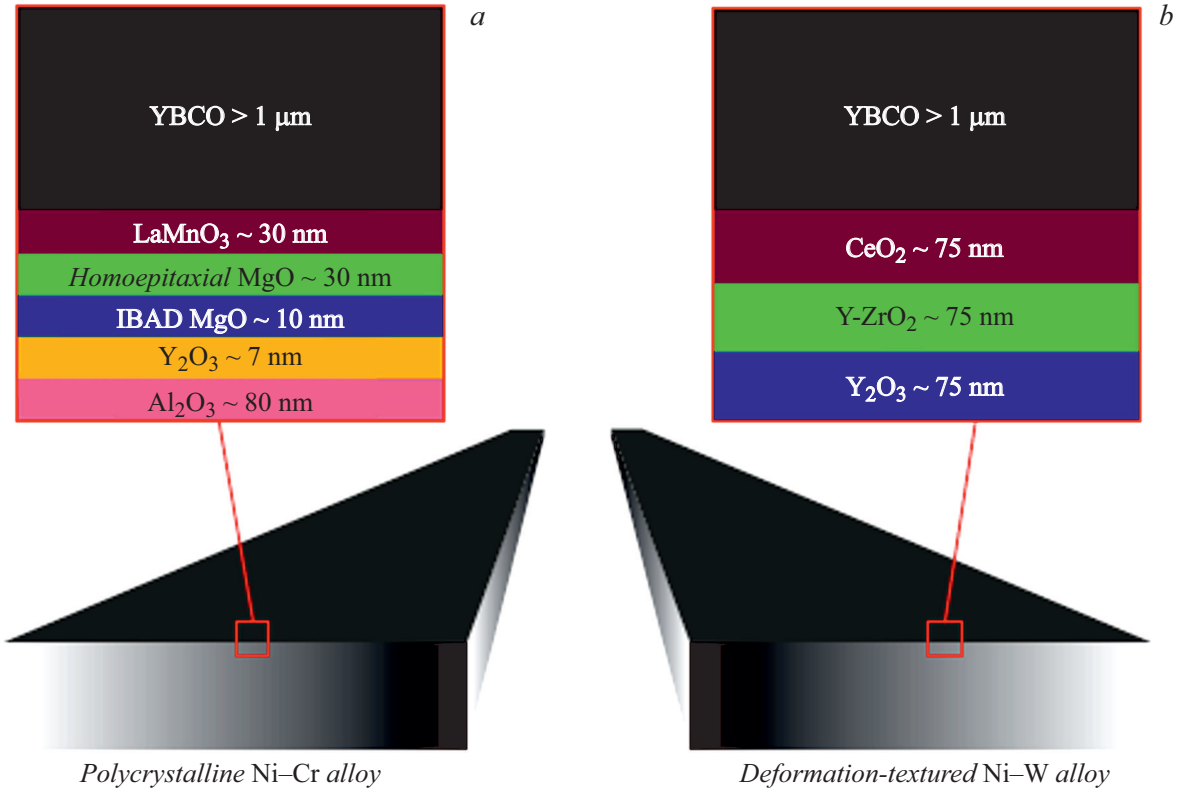

Figure 4. Example of the structure of HTS belts on polycrystalline substrate of NiCr (*a*) and deformation-textured substrate of Hastelloy NiW (*b*) [34]. The figure does not show a layer of silver on the superconductor surface that protects superconductor against interaction with vapors of carbon dioxide.

mechanical damages and direct contact of HTS to shunting material (strengthened copper, stainless steel).

Three methods were proposed for the creation of flexible metallic substrates, whose surface is coated with a layer of oxide having biaxial texture and looking like an elongated mosaic single crystal. Epitaxial growth of Y123 film is possible on such an oxide layer. The first of the methods developed is the Ion Beam Assisted Deposition (IBAD). The second method is the Inclined Substrate Deposition (ISD). The third technological approach proposed is named RABiTS (Rolling-Assisted-Biaxially-Textured-Substrates). The following methods are used more frequently for the application of buffer layers and HTS layer: RCE is the reactive thermal evaporation, PLD is the pulsed laser deposition, PVD is the physical vapor deposition, MOCVD — metal-organic chemical vapor deposition, MOD is the metal-

Table 1. Parameters of HTS-belts from several manufacturers

Manufacturer	Manufacturing Technology	Substrate Thickness, μm	Thickness of stabilizing copper layer, μm
AMSC	RABITS/MOD	75 (NiW)	60
Fujkura	IBAD/PLD	75 (Hastelloy)	20
Shanghai SC	IBAD/PLD	40−50 (Hastelloy)	10
SuNAM	IBAD/RCE	60 (Hastelloy)	20
SuperOx	IBAD/PLD	40−60 (Hastelloy)	2−40
SuperPower	IBAD/MOCVD	30−50 (Hastelloy)	5−20
SWCC	IBAD/MOD	100 (Hastelloy)	40
Theva	IBAD/PLD	50−1000 (Hastelloy)	10−20

organic decomposition. Descriptions of different procedures cab be found in the monograph [35], as well as in the review paper [36].

Neither of these methods use silver as a substrate. Moreover, application of each of these methods enables producing materials, whose critical density of current reaches the values, which are specific for Y123 films, applied onto single crystalline oxide substrates, e.g. strontium titanate. Selection of a method for substrate production and deposition of superconductor layer becomes crucial, since it defines the ratio between the cost and performance of a superconductor, and, finally, success of the technology implementation into production in series for large-scale commercialization.

We can easily see that the cross-section of superconductor is only a small part of the total conductor's cross-section. It is more specific for the 2G belts, where the HTS film layer is equal to the value about 1 μm at the thickness of the metal substrate only of 50−100 μm. Eventually, the superconductor cross-section area in the 1G belts usually does not exceed 30%, and it is less than 2% in 2G belts. In this case it makes sense to talk about not the HTS-material's density of critical current, but so-called engineering (or structural) current density, which is calculated as the ratio between the value of the transport current and the total cross-section area of the belt. It is true that despite the values of critical currents of polycrystalline Bi2223 and film Y123 at $T = 77$ K differ by more than one order due to significant difference in filling coefficients, the engineering current density for the 1G and 2G HTS is virtually the same.

So, the difference between the 1G and 2G HTS-belts is not based on the use of different materials, but on the application of radically different technologies. Today, these two ways are parallel ones. As for today, the first generation materials have a higher structural density of the current and higher energy losses in variable field at lower cost. The second generation materials are considered as more promising in view of their use in strong magnetic fields and for alternating current.

Hereinafter we will discuss the second generation belts only.

REBCO belts in English literature are also called „Coated Conductors" or CC-belts, which can be translated into Russian as „Coated Conductors", however, there is no now steady equivalent term for the „Coated Conductors" in Russian. Instead, Russian literature uses the terms that have already been mentioned earlier, i.e. „second generation belts" or „2G-belts". In the event that finish copper coating is absent, the belts are treated as non-stabilized. The belts with copper coating are often called stabilized. As it has already been noted, the REBCO layer is applied onto metallic substrate through a series of thin buffer layers, as shown in Fig. 5 [37,38]. Wherein the metallic substrate is acting as a textured template [37]. Usually, the thickness of HTS-layer is only 1−3 μm. Therefore, regardless of a high density of critical current of the HTS layer itself — more than 10^{10} A/m^2 at 77 K — the engineering current density, which refers to the current divided by the total cross-section of the belt including a substrate and protective layers, is far less — about10^8 A/m^2.

REBCO belts have more mechanical strength versus three-dimensional materials because of the presence of metallic substrates. However, there is a minimum bending diameter, which means that winding below that diameter will result in the decrease of the belt's critical current. This minimum value of the bending diameter depends both on the architecture of certain belts, and on the belt winding method: superconductor to the inside or to the outside. Generally, one may consider that for this moment the minimum bending diameter of the commercial belt is about 20 mm [39].

Table 1 includes several manufacturers of HTS-belts and technologies they use (according to the work [40]).

Single belts do not fit for magnetic and magnetic levitation applications due to a low volume of the HTS material. This is why HTS-belts are collected into stacks, which may consist of several dozens of separate belts. High values of density of critical current and relative affordability

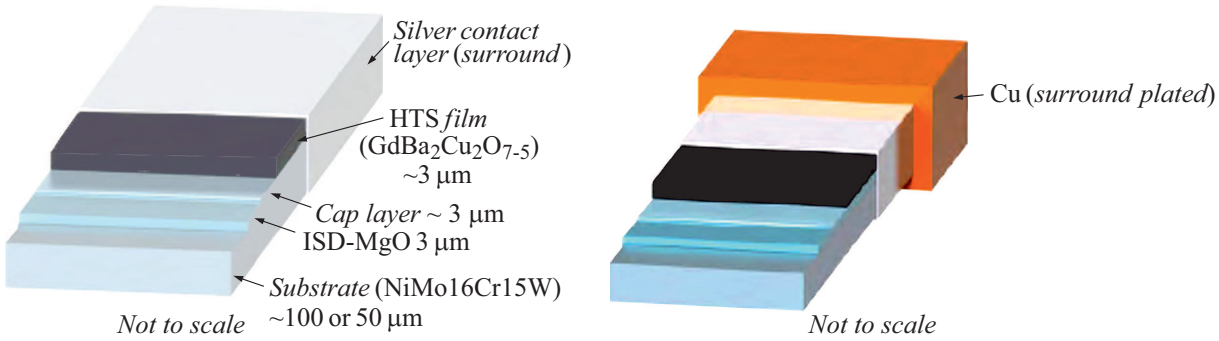

Figure 5. Architecture of an HTS belt manufactured by THEVA [38]. On the left — without stabilizing copper layer; on the right — with stabilizing copper layer.

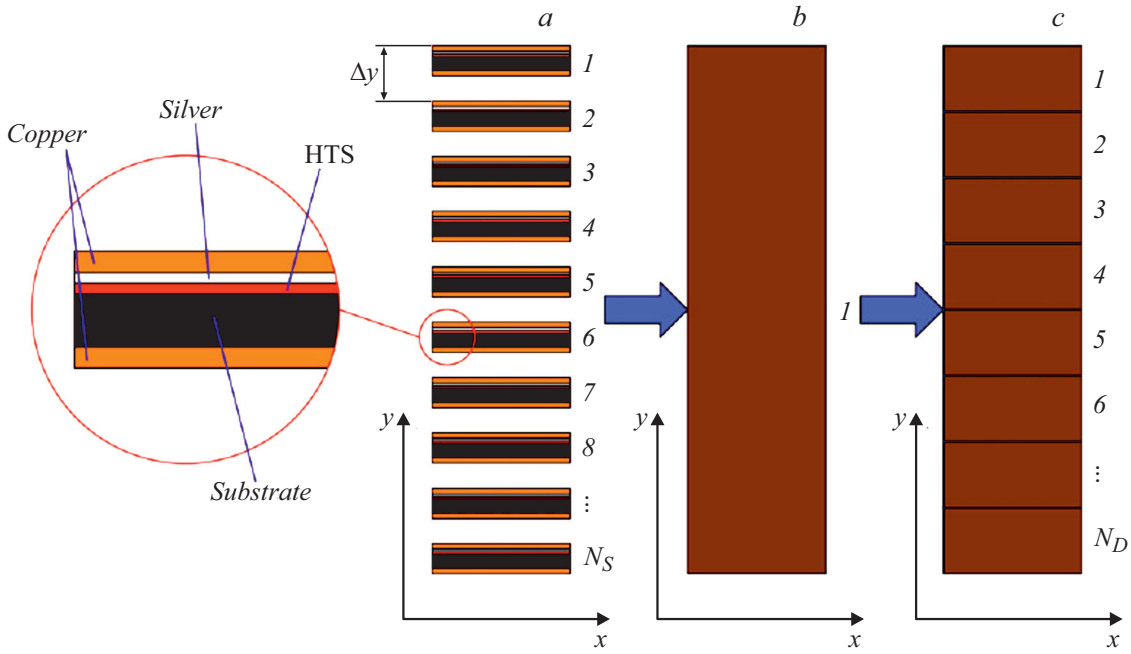

Figure 6. An illustration of the equivalency of a stack of HTS-belts made of separate belt fragments and three-dimensional conductors [48]: *a* — N_s fragments of HTS-belts; *b* — equivalent homogeneous three-dimensional superconductor; *c* — N_d equivalent three-dimensional superconductors of a lower size.

of HTS-belts makes them a promising alternative to three-dimensional ones.

One of the applications of the HTS-belt stacks is capturing the flux generated through magnetization of samples by permanent or pulsed fields. At this moment the properties of stacks of superconducting belts are actively studied [41] (Fig. 6). The maximum value of the magnetic field obtained by using three-dimensional superconductor is 17.6 T [42,43]. But such magnets have problems associated with the brittleness of material, the need for mechanical strengthening, and a low thermal conductivity [42,43], which may cause destruction of a three-dimensional superconductor. Application of the 2G HTS-belt stacks allows to overcome the restrictions imposed by the ceramic brittleness. Availability of a metallic substrate (e.g. Hastelloy) provides high strength to the belt. Thus, e.g., in accordance with the specification of the SuperPower belt, the mechanical stress up to 550 MPa, which corresponds to a theoretical limit in the captured magnetic field 42.8 T, could result in the decrease of critical current by lower than 5% [44,45]. In their turn, the layers of copper and silver (that have higher heat conductivity versus HTS ceramics) are able to rapidly dissipate heat over the whole volume of the belt stack. A union of HTS-belts represents an array of HTS-belts coated with tin-lead solder. Such belts after assembly into a stack are subject to thermal treatment [46], after which the array becomes a single structure, which is convenient for application in real devices. The solder improves thermal contact of adjacent layers in the union, thus making better thermal stability than in case of a belt stack.

Recently it was succeeded to obtain the magnetic field of 17.7 T, captured by a stack of belts [47]. This value

exceeds the record-breaking value for three-dimensional superconductors [42,43]. This fact together with advantages described above allows to say that the 2G HTS-belt stacks are more promising for application in real devices, than three-dimensional HTS.

1.3. Magnetic materials

As a rule, permanent magnets are used for the study of magnetic levitation characteristics. This time, a compound of $Nd_2Fe_{14}B$ (NdFeB), which was discovered in 1983 seems to be the most popular magnets. Detailed characteristics of these magnets, and the methods of synthesis thereof can be found in the works [49,50]. The magnetic moment per formula unit is equal to $32.5\,\mu_B$ at $T = 300\,K$, and the Curie temperature is $T_C = 586\,K$. Magnetic induction (residual magnetic moment) on the surface of a standard magnet $0.5-0.7\,T$, and the coercive force is $1200\,kA/m$. NdFeB is a tetragonal compound with the lattice constants of $a = 0.88\,nm$ and $c = 1.221\,nm$. Virtually all of the Fe atoms are located in the layers, and the Nd and B atoms are in other layers separated by Fe layers from each other. Other rare earth element atoms are sometimes included, in particular, Dy, for the increase of the coercive force in NdFeB. NdFeB crystallites have a high single-axis magnetic anisotropy. There are two main methods of synthesis of NdFeB magnets: baking of powders (in an arc furnace or HF furnace) or pressure casting. In general, the baking method is used, because it is more simple and provides good magnetic properties. However, in cases when complex shaped magnets are required, the pressure casting is preferable.

The shape of used permanent magnets can vary and depends on certain tasks of the magnetic levitation studies. As a rule, these are magnets in the form of a square or rectangular section parallelepipeds or discs of various thickness. More complex configurations, e.g. Halbach arrays [51] are picked up from standard single magnets. The specifics of the Halbach arrays is the magnetic field concentration on the one end of the array and its high decrease on the other end. Moreover, the Halbach arrays provide a high field gradient, which is significant for the magnetic levitation applications. Also, the studies use various concentrators made of low-coercivity material, which may significantly increase the value and the gradient of the magnetic field.

2. Main characteristics of magnetic levitation systems

Let us consider a typical magnetic levitation object consisting of a superconductor and a source of gradient magnetic field — a permanent magnet. For simplicity, let us consider both the magnet and the superconductor have a disc shape with diameters d_{PM} and d_S accordingly. The distance between the planes of the objects is called the levitation gap z.

At the initially coaxial position there are two possible shift options: vertically, along the axis and horizontally — along the plane (lateral shifts). With such movements, the forces emerge correspondingly, oriented by axis (vertical forces) and those oriented perpendicularly to the axis (lateral forces). The vertical force provides the magnetic levitation itself, and the lateral one defines the stability of a magnetic levitation system.

When HTS (or for more general case, the II kind superconductor) is cooled down in the permanent magnet field, the magnetic field, if it exceeds the value of the first critical field, penetrates the superconductor as Abrikosov vortices. In case of change of the relative position of the permanent magnet and superconductor, circular currents are induced in the superconductor, that impede the change of magnetic flux or, as a consequence, initial field, in which it was cooled down. Interaction of these currents with the field of the magnet results in emergence of magnetic forces. If the distance between the magnet and superconductor decreases, repulsive force occurs that impedes superconductor approaching the magnet. If the distance increases — the sticking force emerges that impedes magnet retraction from the superconductor, i.e. after cooling down of the superconductor, both repulsion and sticking forces can emerge in the magnetic field, depending on the magnet movement direction relative to the superconductor. In case of a lateral shift of the magnet or superconductor, the lateral force emerges directed to return the system into position where it is was during cooldown (as we will see further, the lateral returning force emerges only at relative small lateral shifts). All of these results in stable levitation without the presence of additional feedback systems. At that the motion (both linear and circular) of the superconductor along the large set of permanent magnets of the same configuration is going without stop, because the field profile is not changing, therefore, none of the additional forces that would impede the motion occur (except for the air resistance force and braking associated with the heterogeneity of the magnetic field along the motion direction). It is the principle, which the structures of superconductor magnetic levitation transport systems and magnetic bearings are based on.

The factors influencing the characteristics of the magnetic levitation systems are given below.

In order to optimize the lateral force and the levitation force and to guarantee that stability of the developed magnetic levitation systems is provided in any conditions, it is necessary to fully describe these forces. The levitation force can be measured in two modes of the superconductor cooldown: FC — Field Cooled, or ZFC — Zero Field Cooled. As it has been noted earlier, the stable levitation is achieved in the FC conditions. Let us consider the behavior of a magnetic levitation systems consisting of a superconductor initially in normal condition (i.e. its temperature is higher than T_c) and a permanent magnet. In the FC mode the distance z between the magnet and

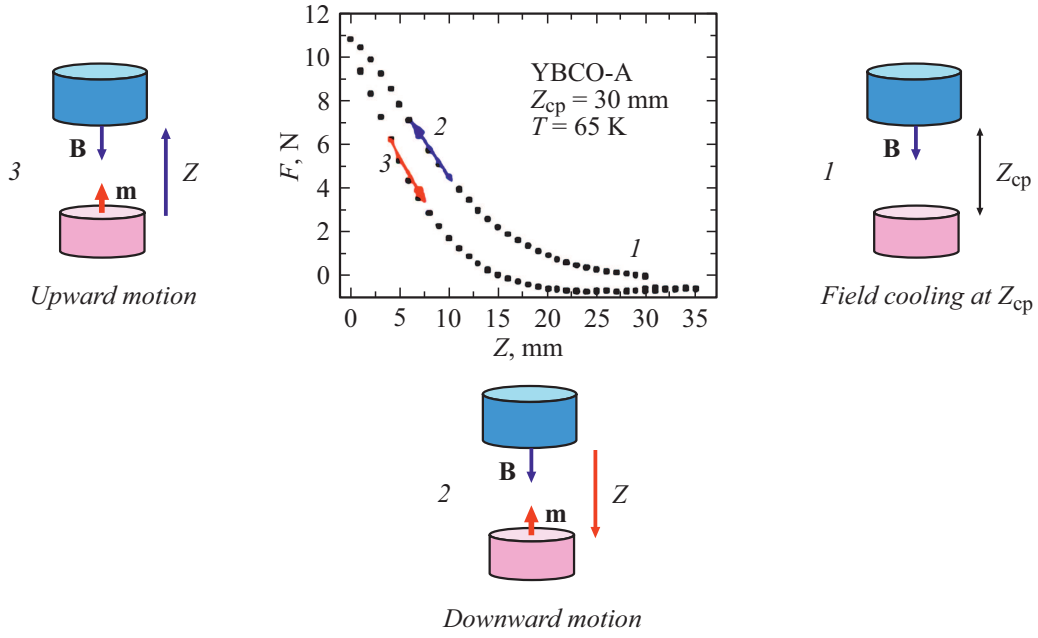

Figure 7. Specifics of movement and measurement of vertical force in case of axial motion (according to the work [52]). At stage *3* the force changes sign, which corresponds to the magnet and superconductor sticking.

superconductor is maintained equal to z_{cp} (cp — cooling position) and the superconductor is cooled down to the measurement temperature $T < T_c$ (spacing *1* in Fig. 7). After stabilization of the temperature depending on the structure of the measuring installation, either a magnetic field source, or a superconductor move vertically, with the decrease of the levitation gap z down to the value of z_{min} (spacing *2* in Fig. 7). In z_{min} the motion direction changes to the opposite one, as a result of which the distance z is increased to the z_{max} (spacing *3* in Fig. 7). During the whole process of the motion the force of interaction between the permanent magnet and the superconductor is registered as function z. In the ZFC mode after cooldown of the superconductor in the field as maximum as close to zero (in practice — at the maximum possible distance from the magnet to the superconductor), the procedure of motions and force registration is the same as in FC.

For the measurement of the lateral force after the stage of cooldown in the field the superconductor is fixed at a distance z from the magnetic field source (Fig. 8). Starting from the position $y = 0$ (axial position), either the permanent magnet, or the superconductor move laterally to a distance of y from the initial position to y_{max}, where the motion direction changes to the opposite one, and the distance is decreased to y_{min}, then the position returns to the initial one ($y = 0$), or, depending on the task, cyclic motions are performed from y_{min} to y_{max} (Fig. 8).

In general, all units for the levitation force and lateral force measurement are similar in terms of their concept. The differences are in which assembly is stationary, and which is moving, whether a magnetic system or cryostat with the superconductor. Also, there are differences in the

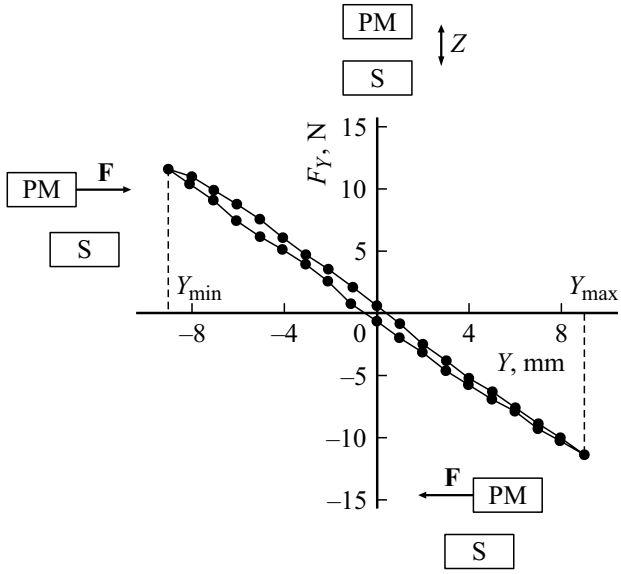

Figure 8. The nature of motion and measurement of vertical force at the lateral movement (from the work [52]).

design of the cool down system. Thus, the stacks cooldown by means of cryocooler is used when studying temperature dependences (Fig. 9).

2.1. Experimental data on magnetic force characteristics of the three-dimensional HTS

Let us consider main factors that determine the levitation force and the lateral force.

— *Effect of the cooldown height in the FC mode.*

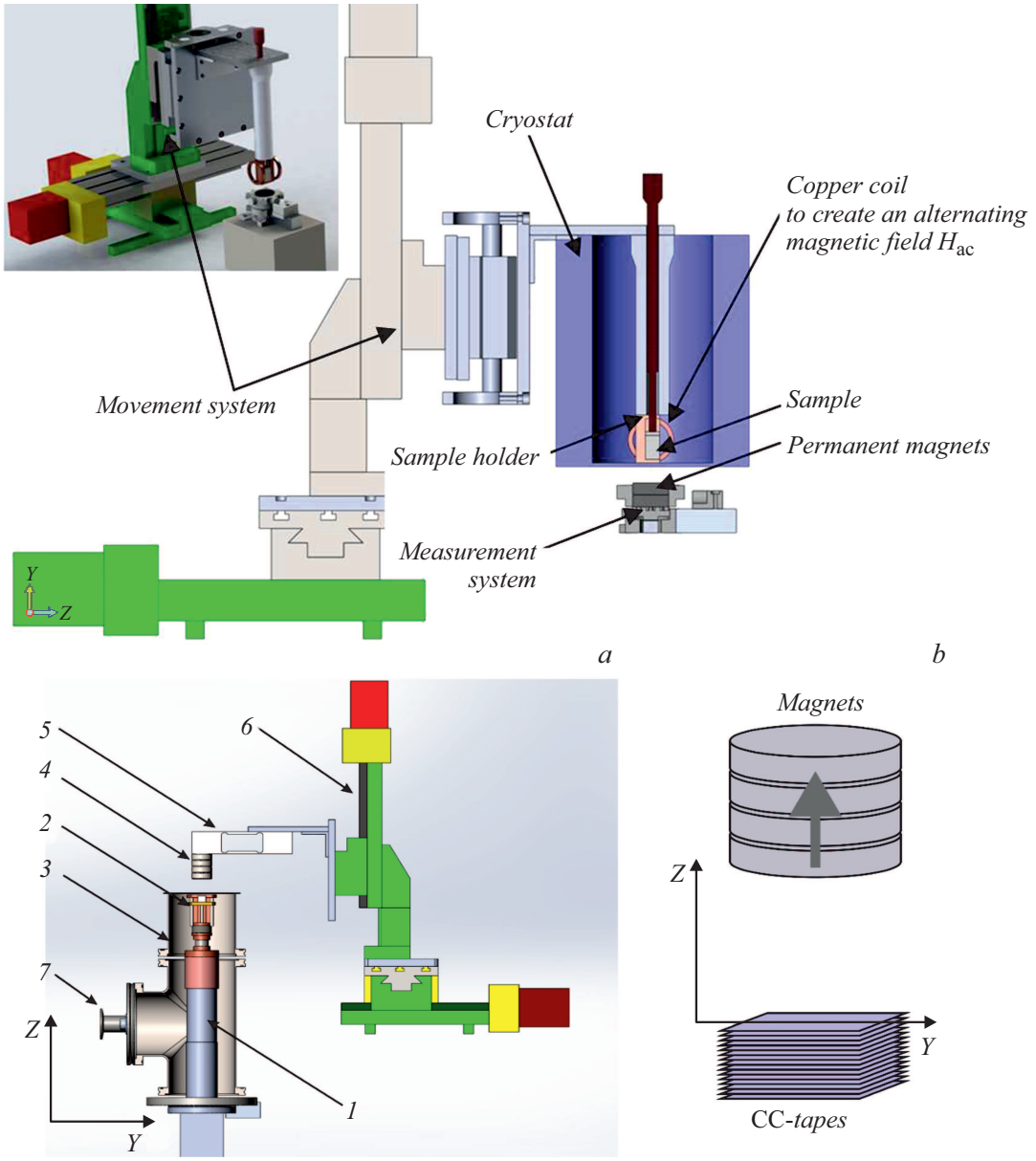

Figure 9. Designs of the measuring system. Top — a small nitrogen cryostat with cooled sample is moving [53]; bottom — the sample is cooled down by means of cryocooler and the block of magnets is moving [54]: *a* — *1* — shank of the cryocooler, *2* — holder of CC-belts, *3* — cryostat, *4* — stack of permanent magnets Nd−Fe−B, *5* — tension sensor, *6* — positioning system, *7* — flange for pumping out and electrical vacuum-tight contacts; *b* — schematic image of mutual arrangement of a stack of CC-belts and a stack of permanent magnets. Arrow indicates direction of the PM magnetization.

The superconductor can be cooled down at various heights relative to the magnet. As noted in [52], the levitation force of three-dimensional YBCO above the Halbach array is the rising function of the cooldown height [55]), meanwhile the measurements of the lateral force in the same conditions [56] have shown that the lateral force is the falling function z_{cp} [48,56].

— *Effect of the permanent magnet diameter.*

In the work [57] the force of levitation was measured between the three-dimensional superconductor YBCO with the diameter $d_s = 18$ mm and permanent magnets with the diameter d_{pm} from 10 to 30 mm. It was shown that the interaction force is rising at start as far as the ratio d_{pm} to d_s is increasing, being the maximum at $d_s \sim d_{pm}$, and then is decreasing at $d_{pm} > d_s$. Increase of the levitation force with the increase of d_{pm} for $d_s > d_{pm}$ is explained by the increase of the portion of the superconductor surface magnetized by the PM field. Further decrease at $d_s < d_{pm}$ is associated with the decrease of magnetic field gradient as far as the permanent magnet diameter is increasing, since the maximum gradient of the field is observed approximately at the magnet edge.

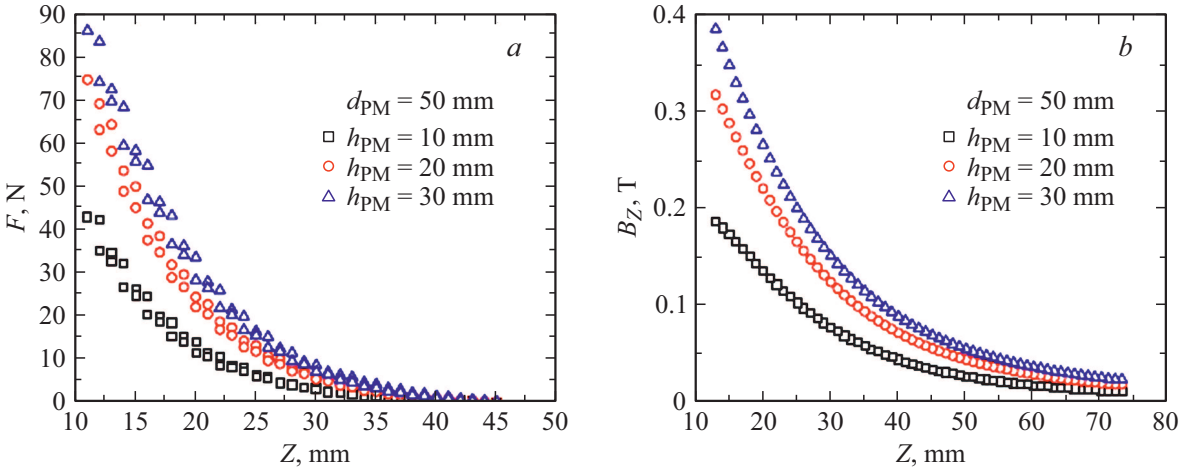

Figure 10. The levitation force for different thicknesses of permanent magnet. The measurements on the three-dimensional magnesium diboride in the FC mode [49]. On the left — dependence of the levitation force on the levitation gap, on the right — dependence of the magnetic induction value on the distance for the magnets with different thickness.

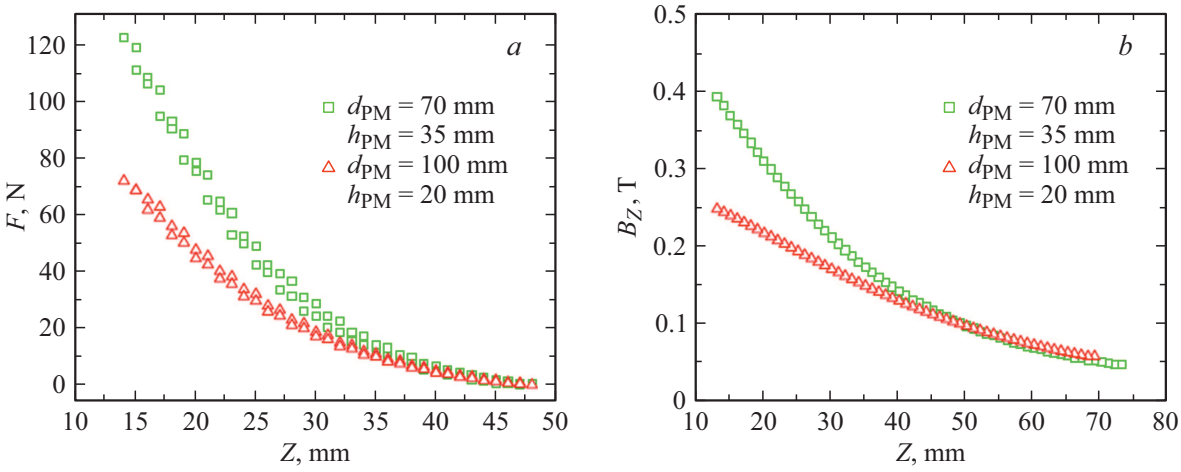

Figure 11. The levitation force and the field value on the axis of permanent magnets with different ratio of the diameter to height [49].

— *Effect of the permanent magnet thickness.*

The results of the studies of the effect of magnets thickness are given in [49]. Analysis was performed when using magnets with the diameter of 50 mm and a three-dimensional superconductor MgB_2 with the diameter of 70 mm. The measurements were performed at 25 K after cooldown of the superconductor in the FC mode at the distance of 45 mm from the magnets. It was shown that the levitation force at start is increasing as far as the permanent magnet thickness is increased h_{pm}, and then it tends to the saturation values, as in the field along the axis of magnets (Fig. 10, *b*). Similar results were obtained for magnets with the diameter of 60 mm.

If the diameter of a permanent magnet d_{pm} is equal or higher than the diameter of the superconductor, then the levitation force is determined by the value of field along the axis of the permanent magnet. It is shown in Fig. 11, *a*, in which the dependence of the levitation force on the distance between the superconductor with the diameter of 70 mm and various magnets is shown at $T = 25$ K: (i) — permanent magnet with the diameter of 100 mm and the thickness of 20 mm and (ii) — permanent magnet with the diameter of 70 mm and the thickness of 35 mm. Fig. 11, *b* shows the levitation force and the value of the field on the axis of permanent magnets with different diameter to height ratio. As we can see, the magnet with the diameter of 100 mm creates both the field and the levitation force far less than that with the diameter of 70 mm. The authors associate the obtained result with an effect of demagnetization factor, which is higher for the magnets with high ratio between d_{PM} and h_{PM}.

— *Effect of the superconductor diameter.*

There is no exact answer to this question. Thus, in the work [49] the levitation forces were measured for a magnet with the diameter of 70 mm and three-dimensional MgB_2 with the thickness of 10 mm with different diameters from 10 to 70 mm. It was shown that the levitation force is the linear function of the variable d_s^3, which the authors

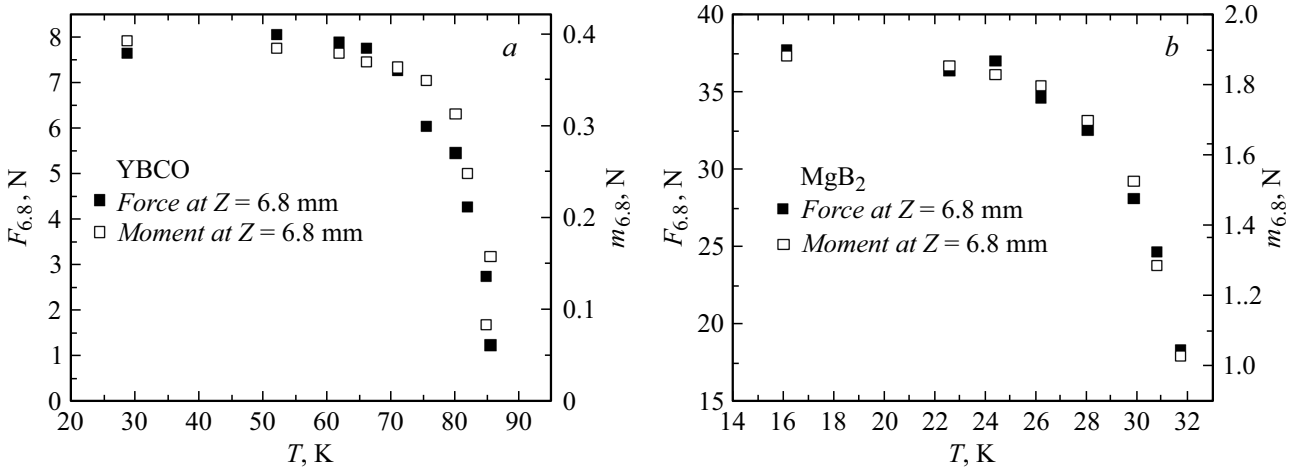

Figure 12. The levitation force and magnetic moment as functions of the temperature for three-dimensional superconductors YBCO (*a*) and MgB_2 (*b*). According to the proceedings of [57].

of the work [49] construed as the force is pro rata to the superconductor volume. With that, the work [57] contains the data indicating that the force is pro rata to the value d_s^2, which means the dependence of the levitation force not on the volume, but on the area of the superconductor. The same as in the [52], the work [49] mentions that dependences of the force on the superconductor sizes do not match the data on the captured field, which, according to the Bean Model [6], is increased as linear function of the superconductor diameter as far as $d_s < d_{pm}$. It is not surprising, because the Bean Model does not consider the dependence of the critical current on the field.

— *Impact of the temperature on the levitation force and shape of the hysteresis loops.*

The temperature impacts significantly the levitation force and hysteresis loops of superconductors. For ZFC conditions, the work [58] has shown that the levitation force of a three-dimensional YBCO increases at start as far as the temperature is falling, and then it tends to saturation. Similar results were obtained in [59] for three-dimensional materials YBCO and MgB_2 in the FC mode (Fig. 12). Saturation is explained by the levitation force approaching to the Meissner limit for large J_c, i.e. a situation, when currents are flowing only by the superconductor surface [60,61]. It should also be noted that the hysteresis loops of the levitation force are high near to T_c and decrease as far as the temperature is falling [58,59].

— *Effects occurring as a result of the use of Halbach array as a magnetic field source.*

It is supposed that the Halbach array provides a higher levitation force than the classical arrangement of magnets. Measurements performed in the [62], confirm this point of view. The work compared the levitation force between two types of sets of magnets (classical and Halbach's) and an assembly of seven YBCO-blocks with the diameter of 30 mm and the thickness of 18 mm, cooled by the field at the distance of 30 mm from magnets. It is seen that the use of the Halbach array results in a higher levitation force (Fig. 13). However, the work [63] noted that if a rectangular superconductor overlaps the whole surface of a set of magnets, the magnets arrangement other than Halbach's could result in a higher levitation force versus the Halbach's one. In any case the Halbach array ensures better stability. Apparently, determination of the best option of the use of a set of magnets is possible only by taking into account certain shape and characteristics of the levitating superconductors as it was done, for example, in the [64].

— *Effect of vibrations and periodic vertical and lateral shifts for the value of the magnetic force interaction.*

The presence of vibrations and cyclic shifts can be a serious problem when designing real magnetic levitation systems, because these processes, along with relaxation of the levitation force caused by the attenuation of the magnetic flux, could cause a high impact on the vertical and lateral forces.

The work [65] studied static and dynamic relaxation of the YBCO and GdBCO discs moving above a set of magnets with different speeds. It was shown that the levitation force is decreasing while the superconductor is in motion, but restores the value, which differs slightly from the expected one at static relaxation, when the speed returns to zero. The force attenuation is more clear when the superconductor speed is rising. Authors believe that it can be explained by faster fluctuations of the magnetic flux applied to the superconductor with high speeds.

Effect of lateral shifts for the levitation force of the YBCO discs hovering above different guides was studied also in [66], where in all cases it was found considerable decrease of the levitation force. Similar measurements in static conditions were performed in [67] on the assembly made of four three-dimensional superconductors YBCO. The levitation force has fallen rapidly within the first several seconds after lateral shift, then the decrease rate was decelerating. If superconductors were cooled down in the

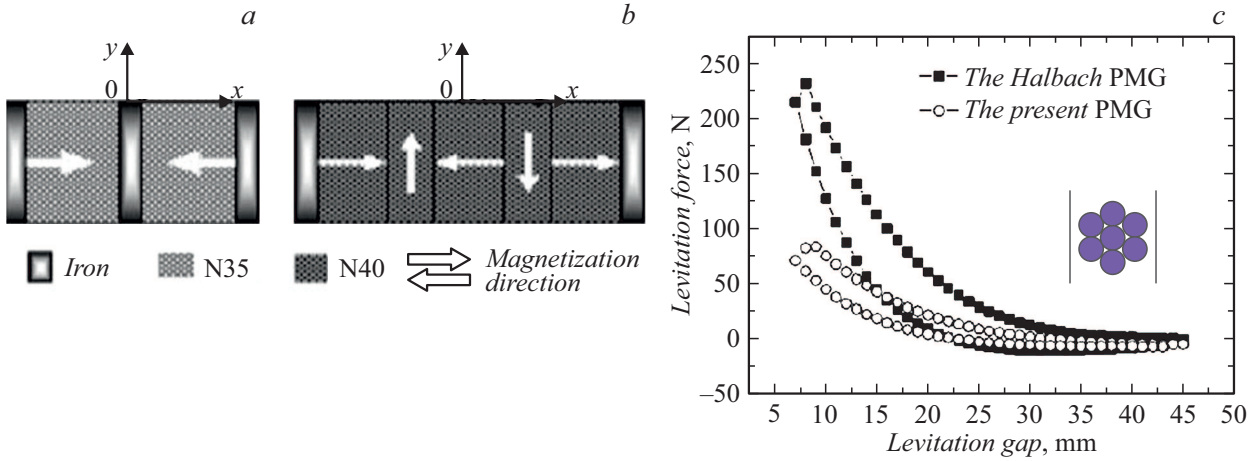

Figure 13. Comparison of the levitation force (c) in cases of classical arrangement of magnets (*a*) and the Halbach array (*b*). According to the proceedings of [62].

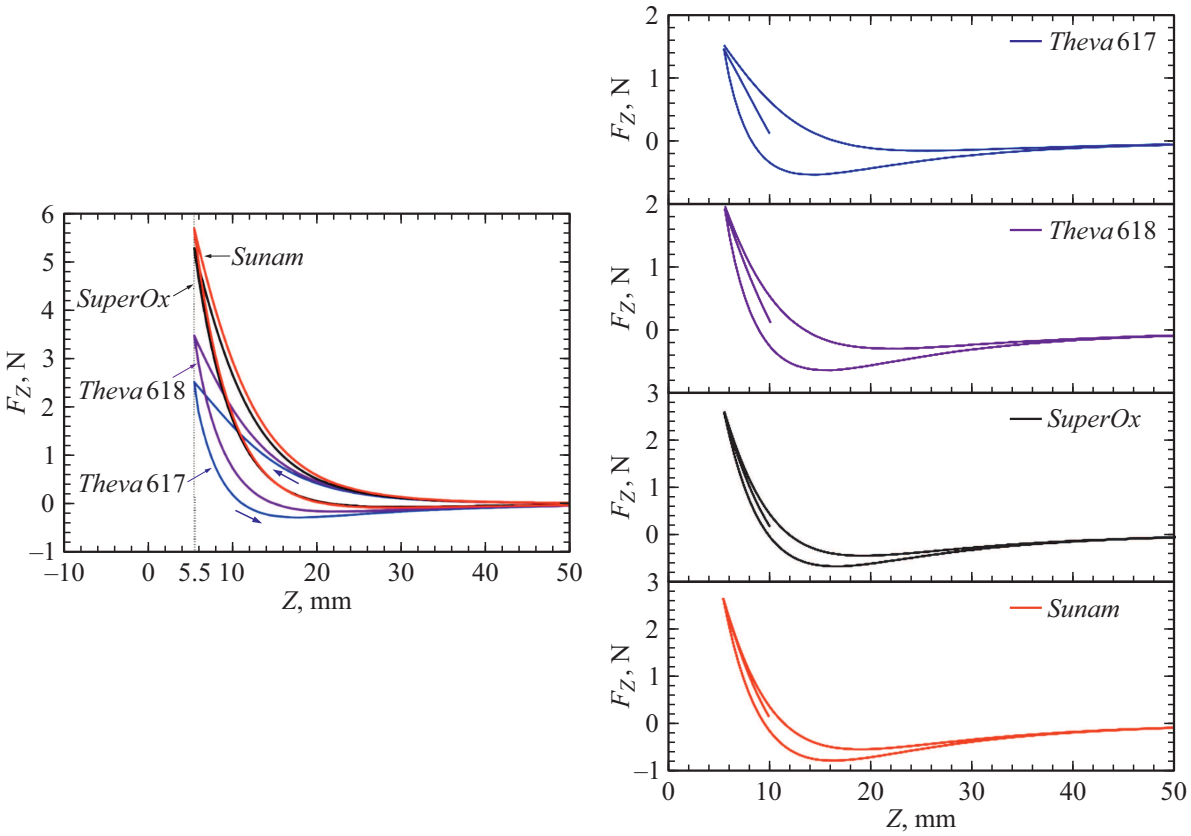

Figure 14. On the left — dependence of the repulsion force F_z between the stack and permanent magnet on the distance between the magnet and superconductor with cooldown in the magnet field (at the distance of 5.5 mm). There are results for stacks of 100 layers. Top curves correspond to approaching of the magnet to the stack, low ones — to the magnet going out from the stack. $T = 77$ K. On the right — cooling mode in the field 10 mm higher than the magnets in the area 0.22 T. Figure shows dependences of the repulsion force F_z between the stack and permanent magnet on the vertical coordinate Z when the belt stack is approaching–leaving the magnet. Results for the stacks of 100 layers. Legends to figure show belt manufacturers. $T = 77$ K. From the work [77].

field, the levitation force modulation by the shift amplitude was opposite to that observed during cool down in zero field. In ZFC the levitation force decrease was the rising function of shift. In case of cooling down in the field the levitation force was decreasing at start and then it rose. Lateral force in FC was the rising function of the shift amplitude, meanwhile it has shown more complex behavior during cooling down in the zero field. With the same shift

the returning force in the field cooling down conditions was always higher than in the zero field cooling down.

The study of effect of vertical oscillations with the frequency of 1 Hz for levitating position of an assembly of three-dimensional HTS and a Halbach array was performed in [68]. Authors concluded that the nature of the levitation force relaxation virtually does not depend on the presence of oscillations, and they concluded that the levitation force relaxation is determined generally by the attenuation of the superconductor magnetization. The work [69] studied hysteresis losses and shock-absorbing properties of a real magnetic levitation system in case of vibrations of various amplitude within the range of frequencies from 2 to 16 Hz. It was shown that at low amplitudes of oscillations hysteresis losses had a low dependence on the frequency, meanwhile the increase of the oscillation amplitude resulted in the increase of hysteresis losses as far as the frequency rises.

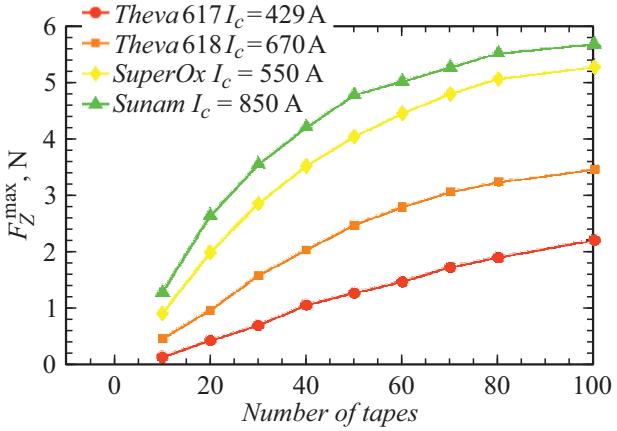

Figure 15. Dependence of the maximum repulsion force on the number of belts in the stack for the belts from various manufacturers. The measurement temperature was 77 K. From the work [77].

2.2. Experimental studies of the magnetic levitation characteristics of the stacks of HTS-belts

For the first time the possibility of application of belt HTS assembled in blocks was indicated by the authors of works [70,71]. These publications presented comparison of the magnetic levitation characteristics of three-dimensional HTS blocks and stacks of HTS belts of the equivalent total thickness. The dependences of the levitation force and of the lateral force were measured both as in a simple geometry of the disc magnet-superconductor, and in the geometry like the Halbach array, as well as the levitation force relaxation. In general, the authors of [70,71] mentioned that behavior of three-dimensional HTS and stacks of HTS belts is approximately the same. These works induced the study of magnetic (study of the stacks magnetization possibility [42]) and magnetic levitation characteristics of the stacks of HTS belts.

The possibility of creation of HTS sets of any configuration determined the direction for many studies aimed at the optimization of the mass-size parameters of the magnetic levitation systems based on the stacks of belts. Further, the studies were also performed for impact of both external parameters (variable magnetic fields, temperature), and internal ones — the value of critical current of separate belts.

2.2.1. Dependence of the levitation force on the thickness of the stack

Our group performed a series of magnetization studies and levitation properties of stacks of the HTS belts. Thus, it was identified that as far as the number of elements in the stack increases, the value of captured field is rising linearly only for a small number of layers (5–10) and approaches to saturation for the stack that contains more than 100 layers (up to 150) [72–74]. With further increase of the number of layers the magnetic field is rising a bit. The data were obtained indicating that the use of HTS-belt stacks in the levitation systems is very promising. Dependences of the levitation force on the distance to the permanent magnet were measured when cooling in the field (FC) and when cooling in the zero field (ZFC), the comparison between the levitation force relaxation and the captured field relaxation was presented. For the creation of real levitation devices it is important to know the effect of parasite vibrations and external variable fields for levitation properties of a superconductor. The work [75] presented results of the study of impact of fluctuations on the magnetic flux relaxation in the HTS belt stacks. It is shown that oscillations with the frequencies up to 30 Hz have no impact on the levitation force relaxation rate. The work [76] studied the effect of crossed magnetic fields for the levitation force. It was shown that with the increase of amplitude of external magnetic field the relaxation rate is rising linearly. Increase of the frequency of the applied field at the unchanged amplitude results in considerable decrease of the relaxation rate.

Detailed studies of the effect of critical current for the magnetic levitation characteristics in various cooling modes were performed in [77]. In this work, the levitation force was measured by using the example of HTS-belts made by different manufacturers, and differing by critical current and the substrate thickness (therefore, by engineering current density — the current divided by the total cross-section of the belt). It was found that a higher critical current corresponds to a higher levitation force. Moreover, the levitation force with higher critical current tends to saturation for a lower number of elements in the stack (Fig. 14–16).

High dependence of the levitation force on the value of critical current induced detailed studies of the temperature effect for the magnetic levitation characteristics, since the critical current is rising as far as the temperature is falling. Thus, the work [54] dealt with both experimental and

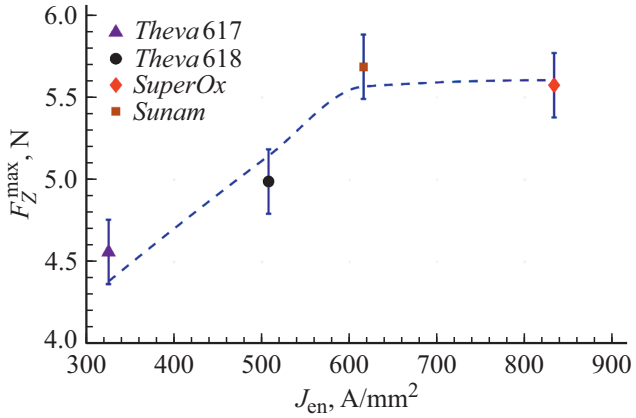

Figure 16. Dependence of the maximum repulsion force on the value of engineering density of critical current in the belt. Built on the basis of the data of measurements in the field cooling mode for the stacks with the thickness of 100 elements made by different manufacturers. The measurement temperature was 77 K. From the work [77].

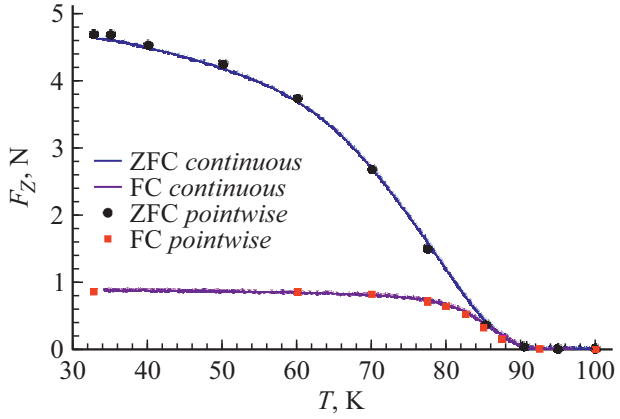

Figure 17. Dependence of the maximum repulsive force on the temperature in the field cooling mode (FC) and in the zero field cooling mode (ZFC). There are results for a stack of 50 belts manufactured by Theva, sample Theva 618. The curves with dots (ZFC and FC) refer to the data of point-by-point measurement with temperature stabilization and heating at every point. Solid curves (ZFC (heating) and FC (heating)) were measured when a sample was approached to the measurement point at the minimum temperature and heating of the sample. From the work [54]. Note that in the ZFC mode the maximum repulsive force is far higher versus to the FC mode. However, ZFC mode is not applied in practice due to the absence of lateral stability.

calculation studies of the effect of temperature and number of belts in a stack for the value of the levitation force and levitation characteristics of HTS-belt stacks made by various manufacturers. Measurements were performed in the field cooled mode and zero field cooled mode (Fig. 17, 18). The obtained experimental data and results of numerical modelling allow to conclude that:

1) in case of cooling in the field, when the temperature is decreasing, the difference in levitation forces of belts with different values of the engineering density of critical current falls significantly;

2) in case of cooling in the field (it is the mode, which is practically used in levitation systems to achieve stable levitation), the cooling down below the liquid nitrogen boiling point benefits to the levitation force lower than 10%. However, achievement of such negative temperatures requires a more complex cooling system, and the benefit of 10% for the levitation force is not reasonable in terms of cost of such a complication of the levitation suspension structure;

3) when cooling down in the zero field at low temperatures (below 65 K) the effect of critical current for the levitation of HTS-belt stacks becomes insignificant. At the same time, as far as the number of belts in a stack is increased, the levitation force rises. Therefore, at low temperatures, an increase of the number of belts in a stack will be more efficient than the use of HTS-belts with higher values of critical current;

4) Increase of the number of belts in a stack results in the rise of the levitation force within the whole range of temperatures up to the value N_{sat}, after which the levitation force value stops changing due to mutual magnetic shielding of the belts in the stack. The value N_{sat} falls as far as the temperature decreases for the same sizes of stack and parameters of gradient magnetic field of permanent magnets.

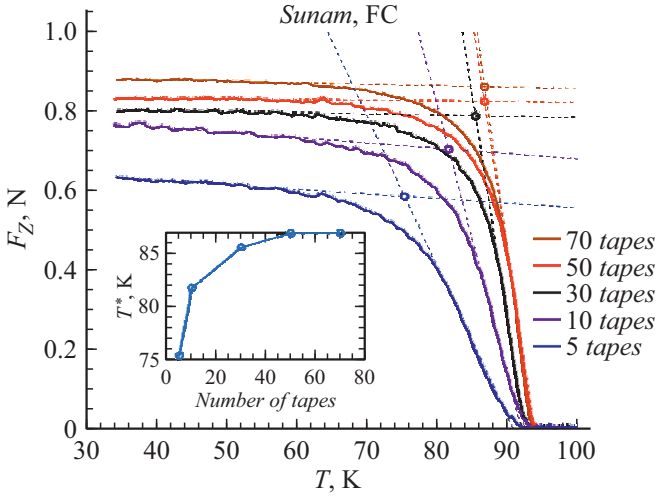

Figure 18. Dependence of the maximum repulsive force on the temperature in the field cooling mode (FC) for various thick stacks made of Sunam belt. Curves were measured when a sample was approached to the measurement point at the minimum temperature and heating of the sample. On the insert— dependence of the crossover temperature T^* on the number of belts in the stack. From the work [54].

The forecast estimates for the numbers of belts from 70 to 700 have determined the values of the number of belts at each temperature, after which the value of the levitation force is not changed. Calculations of the captured flux have shown that the levitation force is reaching saturation

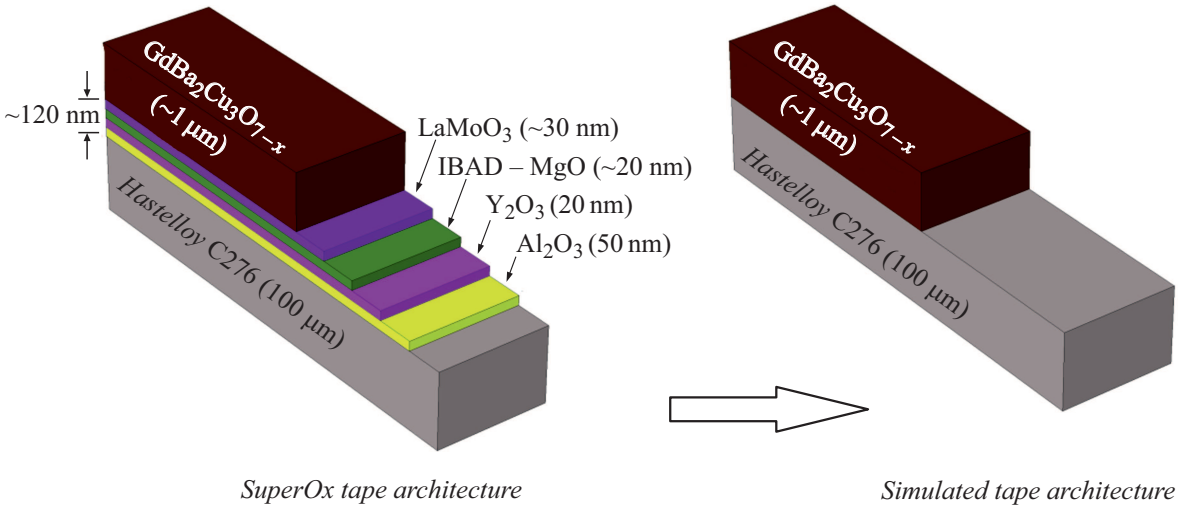

Figure 19. Example of model representation of the HTS-belt geometry.

because of shielding of remote belt fragments in a stack by those closer to magnets.

2.2.2. Dependence of the levitation force and lateral force in case of lateral shifts

The fullest study of forces emerging in case of lateral shifts was provided in the work [53], where practically relevant results were presented, which were absent in earlier publications on the studies of lateral and vertical forces in case of lateral shifts of the GdBCO belt stacks relative to permanent magnets, namely the dependence of the forces on the number of belts (i.e. stack thickness) within a wide range of the number of belts in a stack from 5 to 100, the data on energy losses in case of cyclic lateral shifts. The measurements were performed in the ZFC and FC modes for $T = 77$ K, the effect of lateral shift was measured for shifts within the ranges ± 20 and ± 25 mm. Based on the studies performed the following generalized conclusions were made:

1) the maximum lateral force and the levitation force rise and tend to saturation as far as the number of belts is increased;

2) both vertical and lateral forces depend on the number of cycles of lateral shift and decrease with every cycle. The rate of attenuation initially is rising as far as the number of belts in a stack is increased up to the maximum, which is observed for 30 belts in a stack. Above this value, the forces decrease rate is falling and becomes constant for stacks of more than 40 belts;

3) in case of cyclic lateral shift, both vertical and lateral forces have clearly visible hysteresis, which is decreased as far as the number of belts in stack is increased.

The effect of magnetic field configuration was studied in a series of articles. Generally, all studies are aimed at the selection of a configuration for certain application and have specific goals. As a summary, we can note that the maximum force at close distances is demonstrated by Halbach array, meanwhile at far distances, ordinary sources of gradient magnetic field appear to be more efficient [78].

3. Principles of calculations of magnetic and magnetic levitation characteristics

Calculations play a key role in the studies of magnetic force characteristics for two reasons:

(i) it is impossible to study experimentally all possible configurations of magnetic fields, superconductor assemblies, temperatures and other external conditions for the selection of optimum ones and those required in a certain device;

(ii) calculations allow to determine physical mechanisms of manifestation of magnetic levitation characteristics.

In sect. 3 we describe main approaches to modelling of magnetic levitation systems and perform comparison of the calculation results with the available experimental data.

3.1. Description of a generalized levitation system

As it has already been noted, in terms of physics, levitation is the stable position of an object in the gravitational field without a mechanical support. In fact, in this case the gravity is compensated by the levitation force, which by its nature is the Ampere force:

$$\mathbf{F} = \int_V \mathbf{JB}\,dV,$$

where $\mathbf{F}$ is the levitation force, $\mathbf{J}$ is the distribution of the current densities, $\mathbf{B}$ is the distribution of the magnetic field, and integration is performed all over the volume V of the superconductor.

$$j_c(B, T) = \frac{A}{B} B_{irr}(T)^{\beta} \left(\frac{A}{B_{irr}(T)} \right)^{p} \left(1 - \frac{B}{B_{irr}(T)} \right)^{q}$$

$$B_{irr}(T) = B_{irr}(0) \left(1 - \frac{T}{T_c} \right)^{\alpha}$$

Parameter	*Value*
T_c, K	92
$B_{irr}(0)$ [T]	132.5
($B \perp$ *board face*)	
A [N · m^{-3} · T$^{-\beta}$]	$4.52 \cdot 10^8$
p	0.653
q	2.568
α	1.5
β	1.789

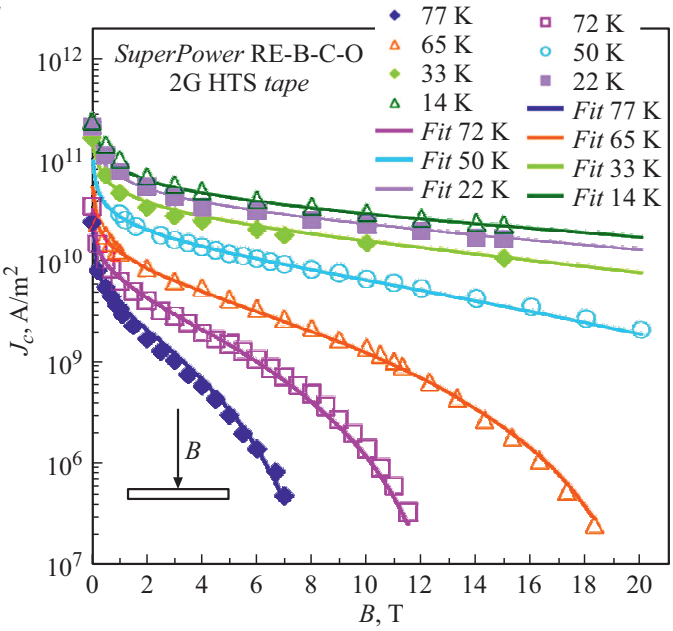

Figure 20. Experimental and calculation dependences of the critical current RE123 of HTS-belts on the field and temperature (figure and table to it were taken from [88]).

We will consider as the levitation system any one, which has interaction of a superconductor with magnetic field. These can be the systems like „superconductor–permanent magnet", „superconductor–current conductor", „superconductor–superconductor" and any possible combinations thereof. Configuration of a levitation system is determined based on the technical and economic requirements of certain applications, where this levitation system will be used. Several examples of the calculation systems with superconductors are given below in subsections devoted to the description of certain model representations. It should be noted that the main focus of this work is at the modelling of systems having practical potential. It means that these calculation models do not cover fundamental phenomena (formation of Cooper pairs, generation of Abrikosov vortices, vortex lattice dynamics, etc.), but describe only the properties of systems within the framework of the phenomenological theory, i.e. have a numerical result, which does not contradict the fundamental theory, but it is not directly derived from that theory. The main goal of such models is calculation and optimization of the system parameters for the achievement of the required engineering characteristics without explanation of internal micromechanisms causing the phenomena observed. In this regard, a part of physical equations is simplified intentionally for the sake of saving expensive computational resources and time without prejudice to the accuracy of end numerical result. Thus, for example, in many cases of calculation of lamellar superconductors functioning in perpendicular magnetic field (the magnetic field is perpendicular to the plane ab), no anisotropy of physical properties in the planes, which are parallel to the magnetic field (axis c), is considered. Next, there are several approaches, which are frequently used for modelling directly the superconductors, in particular, HTS-belts, within the framework of the phenomenological theory.

3.2. Model representation of superconductors

The first simplification, which is the most common one for modelling of the HTS-belt composite-based levitation systems, refers to the simplification of geometry of the calculated system, namely, to the transformation of a real architecture of belts into simplified one that contains a lower number of layers (Fig. 19).

Such a simplification can be done either as dealing with several basic layers of belts (as a rule, the layers of copper, silver, HTS and a substrate) [79–81], or as representation of HTS-belts as thin three-dimensional HTS with engineering critical current [82,83].

In case of superconductors, a unique precise characteristic obtained experimentally and fully describing the properties of HTS-belts is the volt-ampere characteristic (IU characteristic) $E = \rho J$, where E is the electrical field, J is the current density, ρ is the resistance.

However, unlike other layers, for which the resistance linearly depends on the temperature, the temperature dependence of the superconductor resistance is set as a power function:

$$\rho = \frac{\mathbf{E}_c}{\mathbf{J}_c} \left(\frac{|\mathbf{J}|}{\mathbf{J}_c} \right)^{(n-1)}, \qquad (1)$$

where E_c is the critical electrical field equal to $1\,\mu$V/cm, J_c is the critical current, current components $\mathbf{J}$ are calculated based on the Ampere law, n is the index of power depending on the value of magnetic field $\mathbf{B}$ and

Table 2. Fundamental works on the numerical analysis of HTS

Formalism developed (Homemade) or standard software code for calculations		2*D* (two-dimensional system)	2*D* (two-dimensional asymmetric system)	3*D* (three-dimensional system)
A–V	Homemade	[114] [56] [115–119]	[120–124]	[125]
	Software	none	none	[126]
T–Ω	Homemade	[127]	[128] [129]	[130–137]
	Software	none	none	none
H	Homemade	[138]	none	[139]
	Software	[48] [140] [141]	[141] [142]	[140] [142]

the temperature T (the most common reference in English publications is the parameter „*n-value*"). The critical current of belts and the index of power n depend on the temperature and the value of external magnetic field. Therefore, the IU characteristic of HTS is represented like

$$E = \rho(J, B, T)J(B, T). \tag{2}$$

The components of the current density J are calculated based on the master equations of various formulations, which will be discussed hereinafter. In this case the resistance also depends on the temperature, because critical current depends on that. Anyway, as we can see in the equation, any parameter that affects critical current changes the resistance and IU characteristic as a default. This is why the next important step when modelling superconductors is the consideration of various functional dependences of the critical current. It can be the consideration of not only temperature dependence of the critical current, but also the magnetic field dependence (including the angular one), the consideration of anisotropy of critical current, phenomenological consideration of microscopic defects (for example, consideration of the experimental dependence of critical current on the density of the pinning centers) and apparent consideration of macroscopic ones, etc.

There is a series of model approaches allowing to perform consideration with a good accuracy of the dependence of critical current of HTS on the field and temperature. The Kim Model is considered as one of simple approaches to the description of the field dependence of critical current [84,85]:

$$J_c = \frac{J_{c0}}{(1 + H/H_0)}, \tag{3}$$

where J_{c0} is the critical current in own field at the liquid nitrogen boiling point, H is the magnetic field strength, H_0 is the adjustable parameter. The simplest and the most common approach to consideration of the temperature dependence of the critical current is considering it as the following analytical expression [86]:

$$J_c = \beta\left(1 - \left(\frac{T}{T_c}\right)^2\right)^{1.5}, \tag{4}$$

where T is the temperature, T_c is the critical temperature of the superconductive transition, β is the adjustable parameter of the model.

A more complex approach to the description of the field dependence of the critical current was presented within the

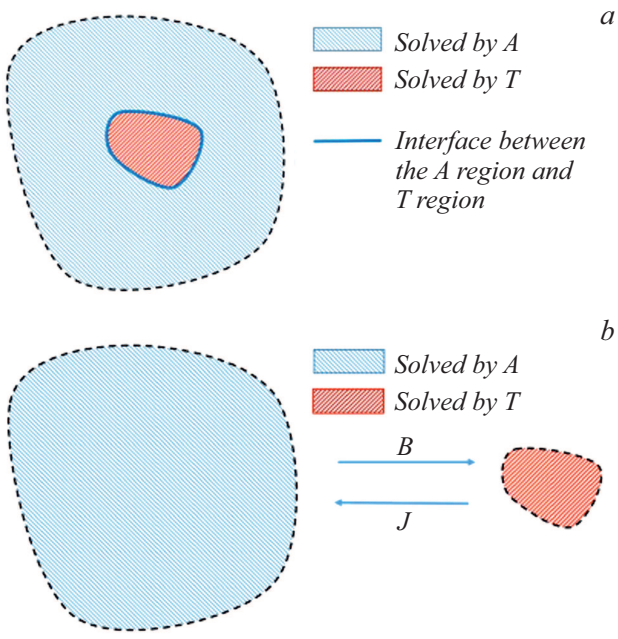

Figure 21. *a* is a link between formulations of MVP and CVP that requires determination of limit conditions at the boundary of contact of the regions; *b* — the tasks of MVP and CVP are solved separately J and the field induction B at every moment of time of the associated solution. Figure from the work [111].

framework of two-exponential model [87], which provides more accurate concordance of the calculation data with the experimental results. There is a series of models, where simultaneous consideration of the temperature dependence and the field one of the critical current is introduced as one analytical expression with fit parameters. An example of such dependence and experimental data for IU characteristics of HTS is given in Fig. 20.

In some models the IU characteristic of HTS is introduced within the framework of the model as interpolation of experimental data, however, since either the critical current itself or variables depending on it form part of the master equations in an independent form, separate consideration of functional dependences of the critical current is still required. The parameter „*n-value*“ of the IU characteristic also depends on the magnetic field and temperature, and in a series of numerical models these dependences are considered [89,90].

Let us proceed with the description of main approaches used in modelling of levitation systems based on superconductors and examples of application of such models for the calculation of certain systems.

3.3. Description of calculation formalisms

There a series of analytical methods for the calculation of the critical state in the superconductor [91–93], however these methods are applicable only for the simplest configurations of superconductors and only in case of homogeneous external magnetic fields. In more complex cases we need to refer to numerical methods. Numerical solutions of Maxwell equations, which together with material equations describing the superconductor state, usually are solved either by means of the finite-difference approximation [94], or by means of the finite-element method (FEM) [95]. The majority of the first works related with modelling of superconductors was done by using original self-developed software. The list of fundamental works devoted to modelling of superconductors and first used formalisms for the description of the HTS behavior under magnetic and current effects are given in Table 2. Over time, separate modular software packages have appeared, which are intended for complex description of many physical processes and have been widely used also for multiphysical description of superconductors. The word „multiphysical“ in this context implies an associated solution of several equations with different master variables (for example, electrodynamic model and heat model, additional consideration of mechanical properties of the system, etc.) The most popular of such modular packages are Comsol Multiphysics [96,97], ANSYS [98,99] and flexPDE [100]. These packages use mainly the finite element method or finite difference method to solve differential equations in partial derivatives. Today, four most common approaches to the description of the superconductors behavior by FEM are in use: H-formalism [101–106], (A−V)-formalism [107,108], (T−Ω)-formalism [109,110], and (A−T)-formalism [111,112]. The

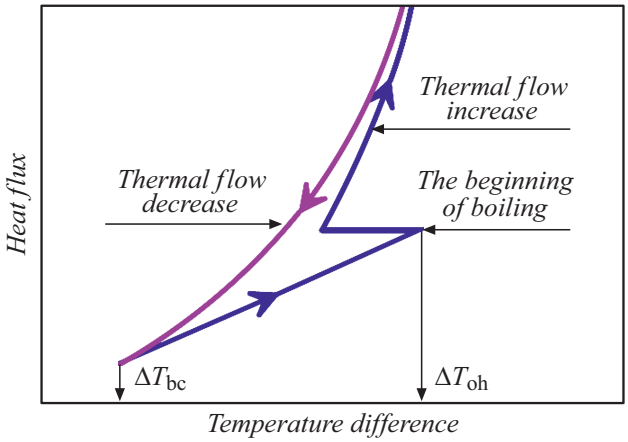

Figure 22. Liquid nitrogen boiling curve subject to boiling hysteresis (ΔT_{bc} is the temperature delay of the beginning of bubble boiling, ΔT_{oh} is the temperature of liquid nitrogen overheating).

word „formalism“ is a common term, which by nature indicates a parameter acting as a dependent variable of the model when solving material equations, like Maxwell equation in this case. Thus, for example, instead of using the term „H-formalism“ it would be more correct to use the phrase „formulation in terms of the magnetic field components“. Despite of the equivalency of these formulations, the methods of solution of relevant equations in partial derivatives may differ considerably [113].

3.3.1. (T−V)-formalism

It is the most stable and fast method of description of the critical state of superconductor featuring the best agreement among the known grid methods. The current vector potential (CVP) **T** is described by the expression:

$$\nabla \mathbf{T} = \mathbf{J}. \tag{5}$$

In fact, the CVP refers to the magnetization of an insulated superconductor. Total magnetic field **H** is calculated as the superposition of external magnetic field $\mathbf{H}_0$ and the field induced by currents in the superconductor **Hs**, superconducting regions are calculated in the formulation of CVP (for two dependent variables T_x and T_y), and non conducting regions — in the formulation of magnetic scalar potential (MSP, variable V). Subject to this expression (5)−(7) the Faraday and Gauss equations are transformed and solved:

$$\nabla \times Hs = J, \tag{6}$$

$$-\nabla V = Hs - T, \tag{7}$$

$$H = H_0 + T - \nabla V. \tag{8}$$

The methodology is applicable for calculations of magnetization of superconductors and processes of the transport current flow, but calculation is performed only for relatively

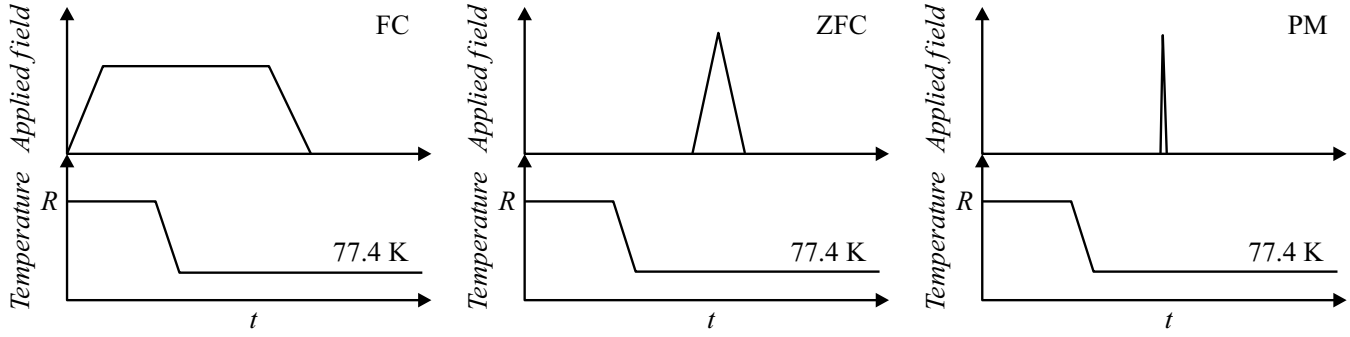

Figure 23. The specifics of mutual modification of external magnetic field and temperature when modelling the cooling modes (R is the room temperature).

simple geometries, such as, for example, an infinite cylindrical superconductor. Such task can be solved analytically, however, by using (T−V)-formalism, one can study more complex loading modes, as well as easily integrate additional equations into the model, for example, perform calculation of superconductor behavior subject to the temperature.

3.3.2. (T−A)-formalism

One of the latest grid methods, whose main idea refers to the use of CVP formulations for superconductive region and the magnetic vector potential (MVP) for non-conductive regions. This methods is applicable to the solution of tasks with a complex geometry; it is quite flexible and efficient. The main problem of the method is correct determination of the continuity conditions along the boundary of the regions division, where different calculation formulations are used (Fig. 21, top). Solution of the problem is spatial division of the regions, at which the regions of different formalisms exchange solutions with each other (Fig. 21, bottom). This requires simultaneous solution of tasks in terms of CVP and MVP. Upon the end of computational process the solutions superimpose on each other for more convenient visualization.

The need for joint simultaneous solution of equations for CVP (for superconductive region) and MVP (for the whole calculation space) requires significant computational resources. However, this problem is solved by replacement of HTS regions with 2D ones without significant loss in accuracy. The work [143] deals with a levitation system consisting of a stack of HTS-belts and a permanent magnet. It is shown that versus the H-formalism, (A−T)-formalism features about 10 times better rate, but it is applicable only to modelling of the systems, where 2D approximation of superconductor is possible. (T−A)-formalism-based 3D model was proposed by a group of authors [111]. Geometry of magnets, ferromagnetic inserts and other elements of levitation system can be represented in 3D, however, superconductor must also be represented as a flat 2D layer. In the work [144] the (T−A)-formulation was applied for the calculation of electromagnetic characteristics of HTS-belt stacks and multiturn coils. Moreover, the work proposed the methods for the improvement of the solution's resolution by applying the methods of multiscale structuring of the finite-element grid. Despite of a good accuracy and efficiency of the methods in some cases, these are not multipurpose ones. Their application is challenging when solving non-stationary tasks or in case of complex geometry of a system. The work [145] performed 2D-calculation of electrodynamic wheel for a Maglev train, which is a magnetic suspension consisting of permanent magnets arranged in a circle and moving over a track made of a superconductive material. The formulation efficiency is shown for the calculation of the buoyancy and traction force based on the wheel motion speed, as well as for the calculation of losses in the system.

3.3.3. (A−V)-formalism

The formalism that implies the use of vector potential $\mathbf{A}$ and scalar potential V as dependent variables for cases when electrical field $\mathbf{E}$ of the superconductor is not parallel to the applied electrical field. At that, the power function for IU characteristic is replaced with many-valued function, therefore, the electrical field $\mathbf{E}$ is represented as a scalar, which imposes the mandatory condition of the superconductor material anisotropy in three directions. The first critical field of the superconductor is taken equal to zero, the Meissner phase is ignored. The Meissner phase in this case implies the presence of superficial currents shielding the external magnetic field and not penetrating inside of the superconductive material until the external magnetic field has achieved the value of the first critical field.

Inside the superconductor the electrical field is induced by the motion of magnetic vortices (so called Abrikosov vortices carrying a quantum of magnetic flux with finite value $\Phi = 2.06783383 \cdot 10^{-15}$ Wb) and parallel to the current density $\mathbf{J}$. This field can be expressed through scalar and vector potentials:

$$\mathbf{E} = -\partial A/\partial t - \nabla V. \quad (9)$$

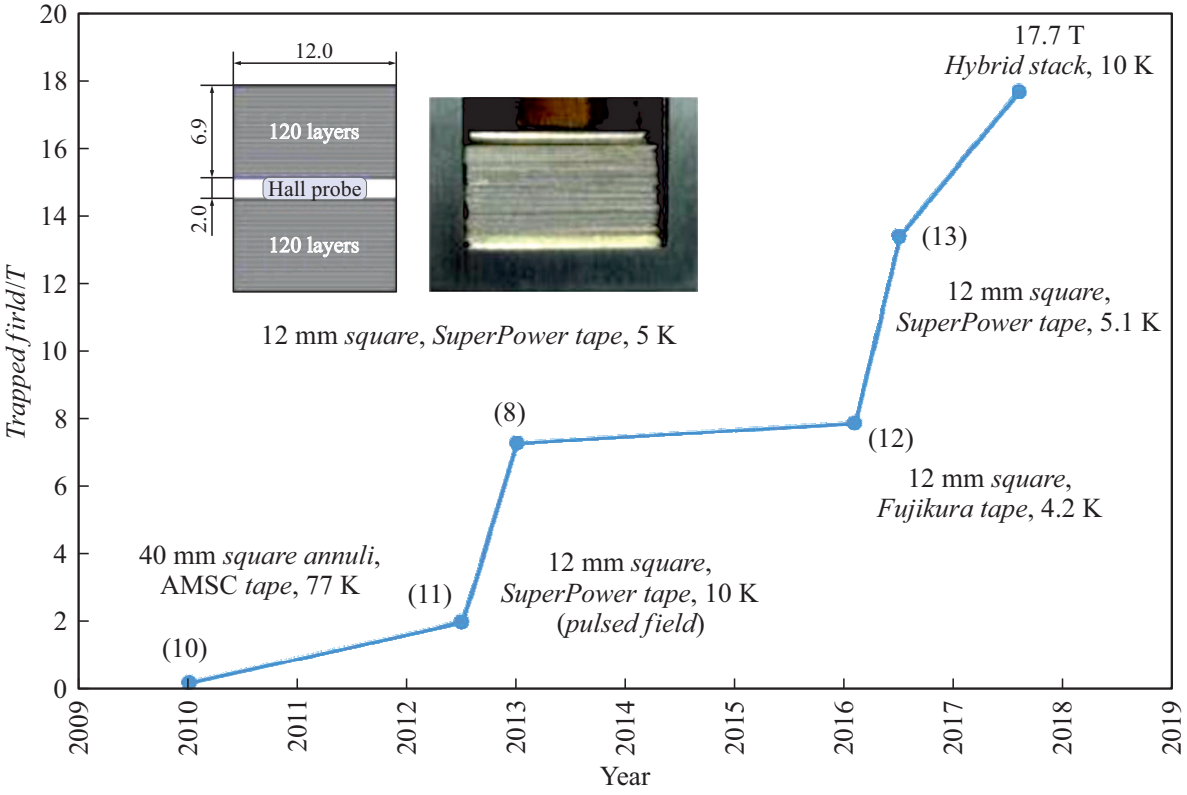

Figure 24. Record-breaking values of the captured magnetic field by HTS-belt stacks [132].

Main part of works represented in the literature with the use of this formalism is devoted to modelling of current limiters and calculation of losses in superconductors. The method is applicable to the calculation of the systems with a complex geometry for the calculation of transport currents induced by external fields, and it is a good alternative for other procedures. The formalism disadvantage is the need for the use of additional integral methods when calculating magnetic fields, which complicates the process of calculations. The work [146] represents calculation of a magnetic bearing implemented by the use of the finite difference method and showing insignificant disagreement with the results of accurate H-formulation implemented by using the finite element method. Calculations show a good agreement with the experimental data both for three-dimensional conductors and for HTS-belt stacks.

It is the most common method and the most complicated one in terms of the agreement, describing critical state of superconductor. Main idea of the method refers to the use of magnetic field as a dependent variable, which allows to avoid cyclic dependence for the current when non-linear dependence of the resistance on the current (see expression (1)) is introduced as a power function for the IU characteristic (see expression (2)), where resistance itself depends on the current. The method is suitable for the solution of tasks in a complex geometry, however, in terms of agreement, it loses against the formulations in the terms T−Ω and A−V, it is more complicated and requires optimization of the calculation algorithms. With that, this method is the most universal one among the proposed, it is applicable to modelling both of processes associated with the transport current flows, and of the processes associated with the induction of currents by external magnetic fields, as well as to complex calculation of sophisticated levitation systems. Since the solution of tasks in the H-formulation requires considerable computational and time resources, in order to simplify the computational process, the mechanisms of adaptation of the elements grid are proposed [147]. The work uses both the above mentioned methods of multiscale structuring of the grid, and of the grid representation, as well as pulling the grid through all layers of the HTS-belt stacks. All four formulations were originally based on the solution of Maxwell equations, however, the H-formalism has been the most frequently applied for the description of behavior of belt superconductors with a high ratio of geometrical parameters of belts. A more complicated task is modelling of behavior of the HTS belt stacks in heterogeneous magnetic fields of complex configurations, since this task may require mandatory 3D setting of the task and direct modelling of the motion processes of magnetic field sources. The work [148] described a combined model of HTS bearing based on the associated (A−T−H)-formulation considering the magnetic assembly rotation.

In some cases, homogenization methods are applied when calculating the levitation systems based on HTS-belt stacks. The idea of the method refers to treating a stack of HTS-belts as a three-dimensional superconductor, wherein relevant limitations are introduced as to flowing of the z-component of currents. This approach was offered for the first time in [149], and then verified and improved in the works [83,150,151]. A disadvantage of the method is the fact that the engineering current density in belts is used when applying stacks homogenization, therefore, it is challenging to consider a lamellar structure of composites and to perform comprehensive heat calculation. The homogenization model treats HTS-belt as a three-dimensional sample with the thickness equal to a sum thicknesses of all layers forming part of the composite. At that, current is flowing within the volume of such HTS, that is equal to the belt's engineering critical current. With that, the model cannot clearly consider the temperature dependences of the electrical conductivity, thermal conductivity, heat capacity, and density of the layers. Note that one of the main features of the homogenization model (an analog is three-dimensional HTS) and a full model of HTS-belt stacks including the lamellar architecture of composites into consideration, is taking of thermal processes into account.

3.4. Modelling subject to thermal processes

The following expression underlies the thermal processes description

$$\rho C_p \frac{\partial T}{\partial t} + \nabla(-k\nabla T) = Q + \rho C_p w \nabla T, \qquad (10)$$

where C_p is the heat capacity at constant pressure, ρ is the density, k is the thermal conductivity coefficient, w is the field of temperature rates determined by parameters of thermal impact and properties of materials (mainly by thermal conductivity and heat capacity), Q is all heat sources. In this case the temperature T acts as a dependent variable when solving the non-stationary task. The calculation considered temperature dependences of heat capacity, density and thermal conductivity for all layers of each belt [61].

3.3.4. H-formalism

Heat release Q in the system was calculated by the formula

$$Q = EJ, \qquad (11)$$

where E is the electrical field, J is the current density.

Distribution of currents J in superconductor is determined by magnetization conditions and is calculated when solving the PDE equations. The temperature dependence of critical current is introduced within the framework of the model in accordance with expression (4), the temperature of critical transition T_c for HTS-belts $GdBa_2Cu_3O_{7-x}$ manufactured by SuperOx, measured experimentally is 92 K.

Simulation of nitrogen cooling refers to specifying the heat-exchange coefficient for a region of space surrounding the HTS-belt stack. As known, there are two specific boiling modes of liquid nitrogen: bubble boiling mode and convective heat exchange mode (Fig. 22).

These modes are characterized in different heat-exchange coefficients. The heat-exchange coefficient for the bubble boiling is calculated as:

$$\alpha_{boil} = C_h q^{0.624} (\rho C_p k)^{0.117}, \qquad (12)$$

where ρ is the density, C_p is the heat capacity, k is the thermal conductivity of liquid nitrogen, q is the heat flow, C_h is the coefficient [62,63].

The heat-exchange coefficient for stationary boiling of liquid nitrogen is determined by the difference of temperatures ΔT at the boundary between a stack of belts and liquid nitrogen and is calculated by the formula

$$\alpha_{conv} = C_{conv} \Delta T^{1/3}, \qquad (13)$$

where C_{conv} is the coefficient from the work [64] depending on the temperature.

Cryocooler cooling down within the framework of the model is performed through a copper array, whose external boundary is set as a cooling source with specific temperature. Heat radiation from external walls of cryostat at the indoor ambient temperature is taken into account. The calculation derives the value of the capacity of cooling element operation, which must not exceed the capacity of a real cryocooler cooling system. Otherwise, the temperature mode is failed, which leads to undesired heating in the system.

Because it is impossible to introduce circular current directly (through the terminals from the current source) into HTS sample, three methods of non-attenuating currents induction are used in superconductive samples:

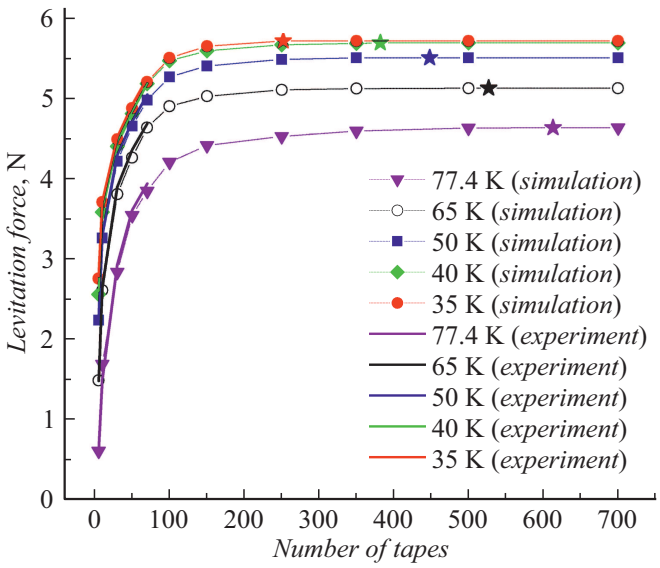

Figure 25. Dependence of the levitation force on the number of belts in a stack [137].

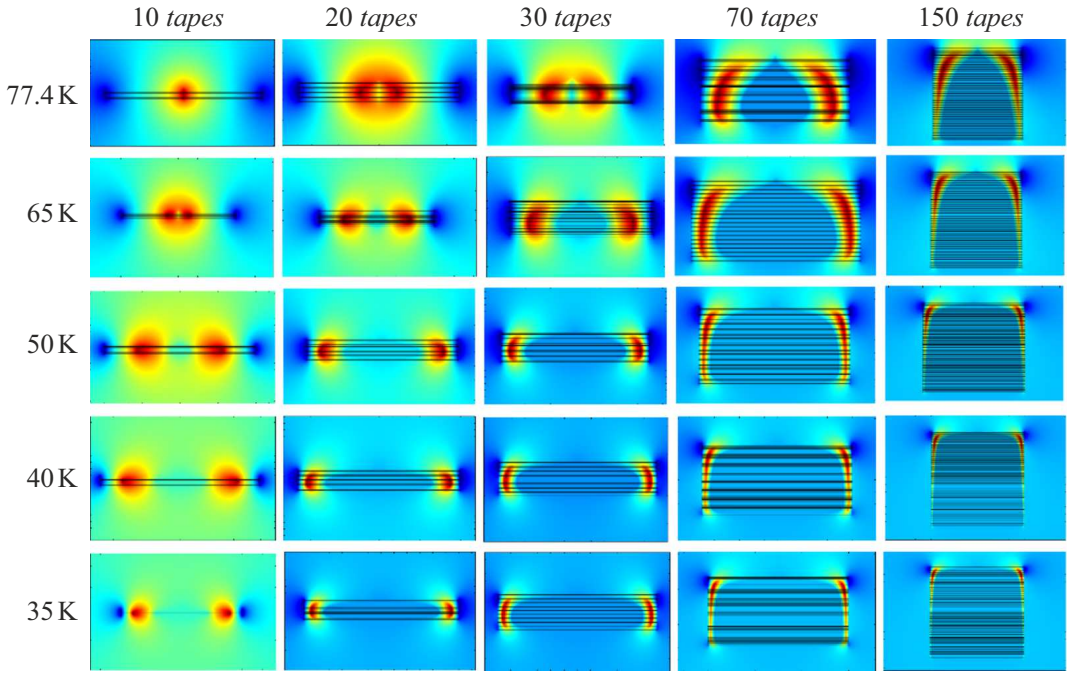

Figure 26. Distribution of captured magnetic flux by HTS-belt stacks at various temperatures [137]. Warmer color shades correspond to higher value of captured magnetic flux.

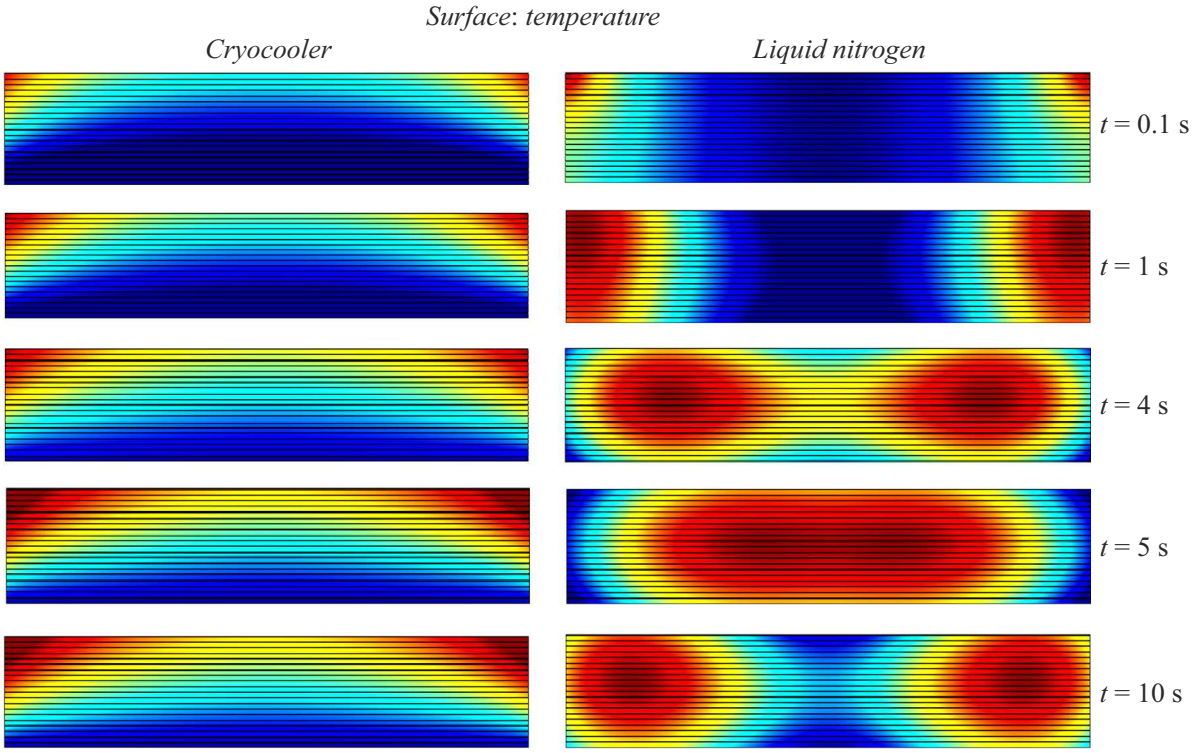

Figure 27. Dynamics of thermal processes in a stack of HTS-belts in case of cryocooler and liquid nitrogen cooling [138]. Warmer color shades correspond to higher value of the temperature. The maximum temperature on the represented distributions was 75.4 K.

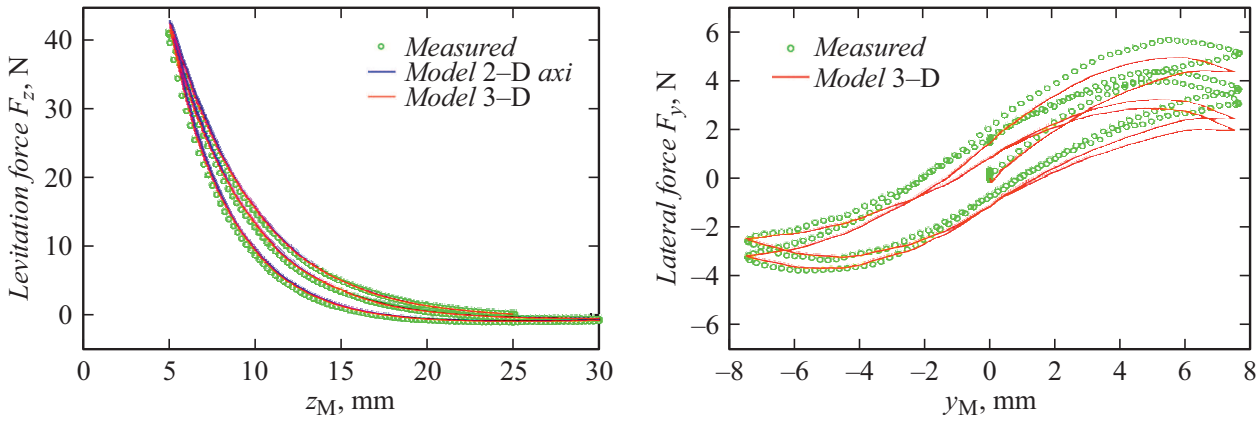

Figure 28. Dependences of vertical (on the left) and lateral (on the right) levitation force on the coordinate [120].

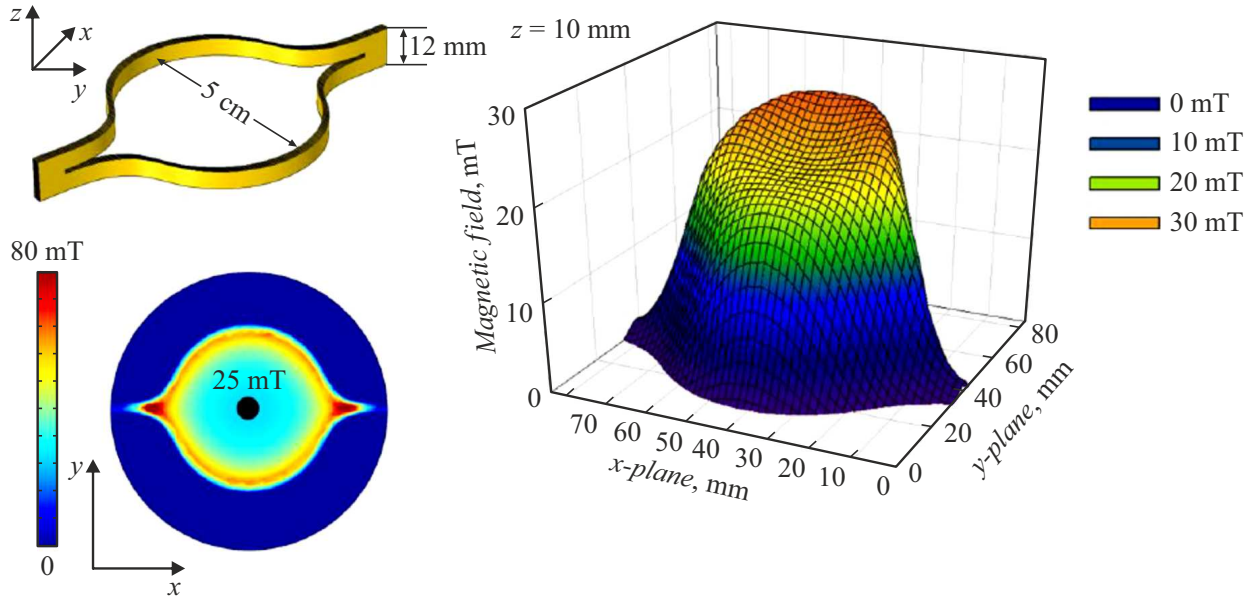

Figure 29. Geometry of superconductive ring and distribution of captured flux above its surface [155].

1) magnetic field cooling;
2) zero field cooling with further slow magnetization;
3) zero field cooling with pulsed magnetization.

The system calculation was performed for the field cooling (FC) and zero field cooling (ZFC) cases. The differences of these modes are shown in Fig. 23.

3.4.1. Magnetic field cooling (FC)

A superconductor heated above the critical temperature is placed into external magnetic field and the temperature is slowly decreased below T_c ($dT/dt = 0.1$ K/min). Thereafter, external magnetic field is slowly decreased down to zero. This method is the most common one for the magnetization of massive superconductors in magnetic field. The field decrease rate must be low enough, so that heat dissipated during the magnetic flux motion can be transferred to refrigerant, thus ensuring isothermal conditions of magnetization ($d\mathbf{B}/dt < 0.2$ T/min). In practice, the decrease of the magnetic field as a result of relaxation (magnetic flux creep) leads to the need for restoration of the initial field value. FC process cannot be applied for restoration of the initial field value, because it requires heating above the critical value. The maximum captured fields (and minimum temperatures of the magnets functioning) are limited to mechanical strength of samples, but not to current carrying capacity of HTS.

3.4.2. Zero field cooling with further slow magnetization (ZFC)

At start, a superconductor is cooled down below the critical temperature, then external magnetic field is applied

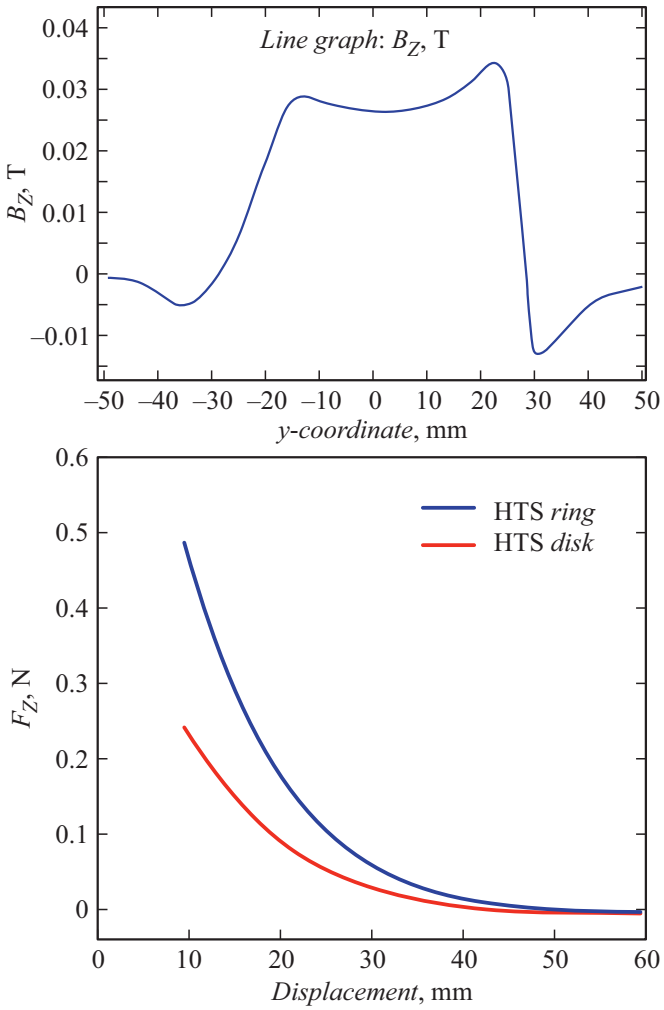

Figure 30. Distribution of captured magnetic flux above HTS-ring (top) and comparison of levitation characteristics of HTS-disc and ring (bottom) [156].

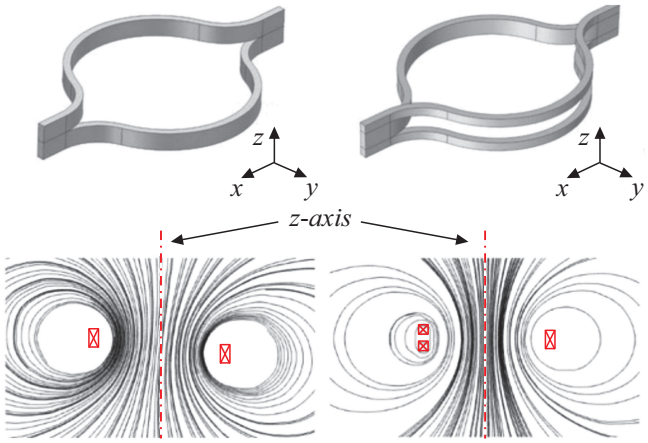

Figure 31. HTS-ring with single cut and double cut (top) and distributions of captured magnetic fluxes corresponding to these configurations (bottom) [141].

thereto, which is rising at start and then it is decreased. When the external field in the superconductor is increased, diamagnetic currents emerge, creating magnetic field oriented oppositely to the external one. When the external field is decreased, paramagnetic currents are induced in the periphery of the sample and creating the field that coincides the direction of the magnetization field. The same as in the field cooling (FC) method, the magnetization field herein is changed slowly — isothermally. Criteria of isothermal behavior are the equality of the heat exchange capacity of a refrigerant (or a cryocooler) and heat radiations in the sample. Specific values of the external field change rate in case of magnetization by the ZFC method are determined by the sample cooling mechanism and characteristics of its materials. Advantages of the zero field cooling method include the absence of the need for heating the sample above the critical temperature prior to magnetization, which could be important when powerful magnets of captured flux are in operation, for whom frequent defrosting is unfavorable.

3.4.3. Pulsed magnetization zero field cooling

The pulsed magnetization is similar to the process of zero field cooling (ZFC), because prior to magnetization the sample is cooled down to the temperature below critical one. But, unlike the ZFC, the pulsed magnetic field with the amplitude of 1.5 T with specific pulse times $t_{imp} = 50\,\text{ms}-0.5\,\text{s}$ is created for magnetization when modelling. The pulsed magnetization is the most promising in terms of capturing the magnetic field when using a series of pulses versus other methods. In contrast to the methods described above the pulsed magnetization is performed in adiabatic conditions, when heat exchange between the sample and the environment can be ignored during the time of pulsed effect because of low pulse duration. It results in that the sample temperature after pulsed magnetization appears to be higher than that of the refrigerant due to HTS-material heating when magnetic flux is penetrating. Therefore, in case of nitrogen cooling it is necessary to consider possible sudden change of thermal characteristics of the refrigerant during heating, and in case of cooling by thermal conductivity of a solid body (cryocooler cooling) it is required to accurately calculate the capacity of cryogenic equipment necessary for keeping the thermal mode.

3.5. Some of the results of calculation models application

As it has already been noted, HTS-belt stacks have a huge potential in view of their application in magnets of captured flux, and magnet bearings for kinetic energy accumulators, levitation suspensions for transport systems, elements of high-speed rotor systems. For the years of existence the values of magnetic flux captured by HTS-belt stacks have

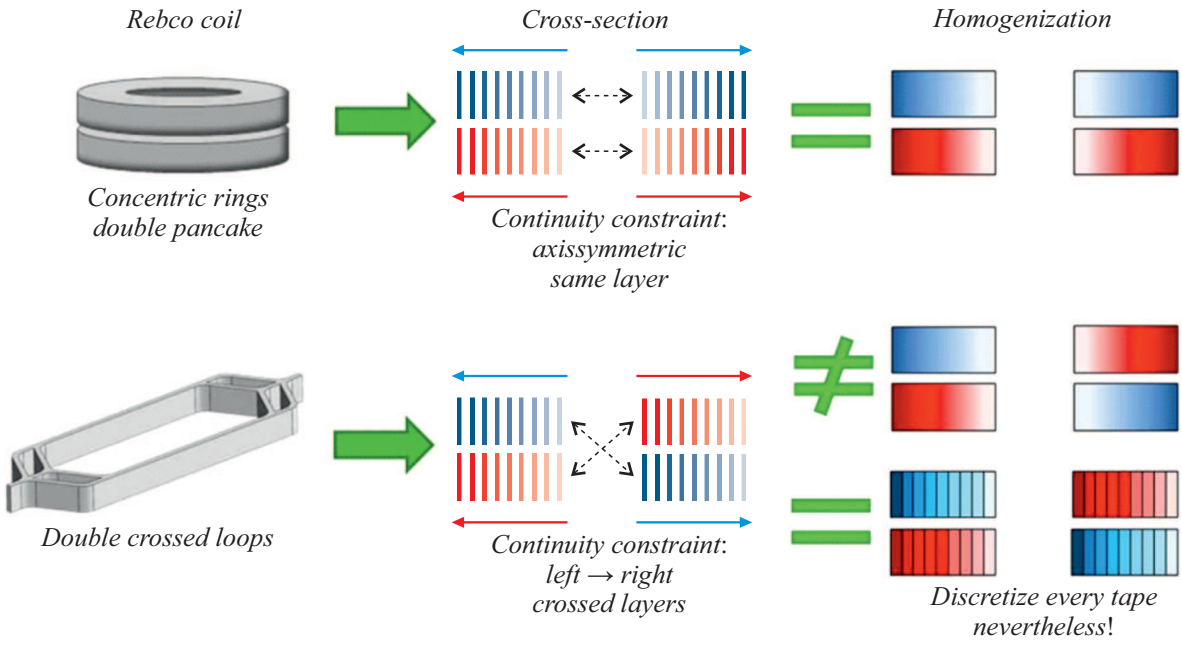

Figure 32. Homogenization of HTS-loop and double wafers [136].

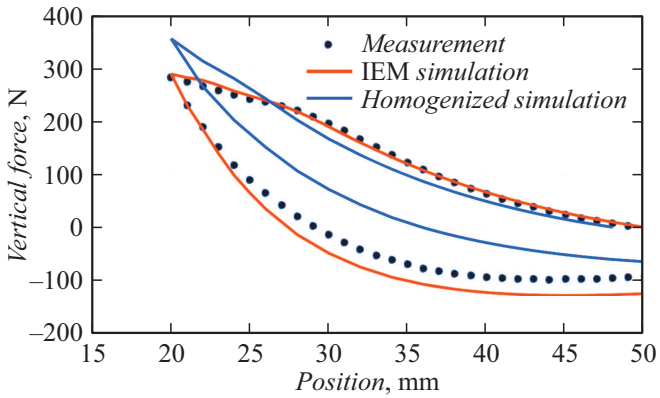

Figure 33. The levitation force for HTS-loop [136].

grown dozens of times (Fig. 24) [47]. The work [47] presents the calculation of a magnet of captured flux based on the HTS-belt stacks with the record-breaking captured magnetic field over 17 T.

The publications include many works presenting the associated electrodynamic and thermal calculations of HTS-belt stacks subject to their layered structure [47,79,152,153]. These works deal with 2G HTS-belt stacks in perpendicular magnetic field [79,152] or superconductive rings as elements of a levitation system [153,154]. For HTS-belt stacks, calculations of current distributions and captured magnetic fields were performed, as well as calculations of levitation forces for belt stacks with the height from 5 to 700 belts in a stack within a wide range of temperatures [54] (Fig. 25). It was shown that a finite height of a stack does exist, so, if exceeded, the value of captured field and levitation forces stop rising, wherein for lower temperatures the limit height of a stack is lower than for higher temperatures and the maximum value of levitation force is always higher. The results of calculation are in a good agreement with the experimental data.

For HTS-belt stacks of different height, distributions of captured magnetic flux were obtained that show specifics of shielding of remote layers of stack by layers located closer to the permanent magnet (Fig. 26) [54], as well as dynamics of distribution of thermal spot when cooling HTS-belt stacks by cryocooler and liquid nitrogen (Fig. 27) [86]. At that, due to a high difference of numerical values, creation of a common colored scale for the presented distributions seems to be impossible, however, these distributions in general demonstrate clearly physical processes occurring in HTS-belt stacks in case of magnetization. On the presented distributions warmer colors correspond to higher physical value.

In the work [141], by the finite element method using the H-formalism, levitation force dependences on the coordinate were calculated at cyclic vertical and lateral shifts in 2*D* and in 3*D* (Fig. 28). The calculations also demonstrate a good agreement with the experimental results. This work presents calculation data for three-dimensional HTS-bearing, as well as for HTS-belt stacks-based bearing by using the homogenization method.

As regards HTS-rings, the work [155] for the first time dealt with HTS-rings as a magnet of captured flux, which by nature refer to a stack of HTS-belts with central cut and located onto a non-conductive former. Asymmetry in the field distribution above the magnet surface is shown (Fig. 29), which later was obtained in the work [156], where

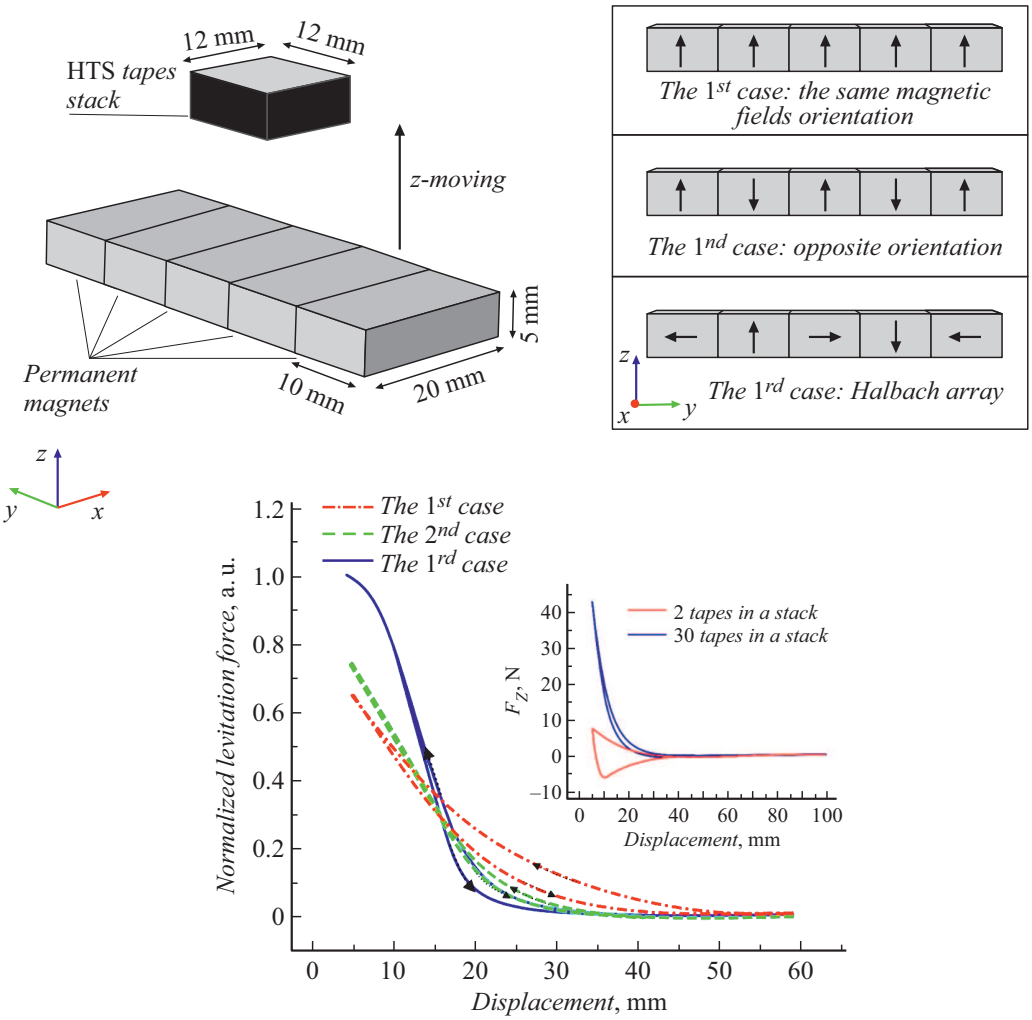

Figure 34. Dependences of the levitation force on the levitation gap value in the HTS-belt stack in magnetic fields of various magnetic assemblies [153].

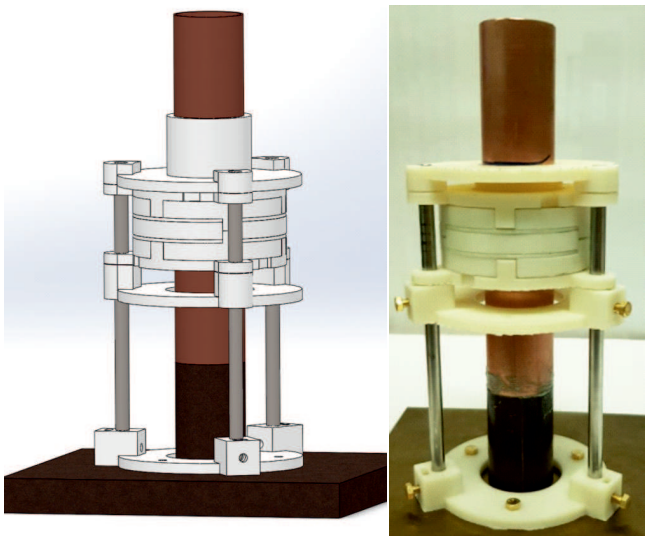

Figure 35. On the left — a design of superconductive bearing, on the right — image of manufactured bearing model [136].

the increment of the levitation force was shown with the use of superconductive rings versus HTS-disc (Fig. 30).

As it has already been shown, when using HTS-rings, there is asymmetry of magnetic flux (Fig. 30) that results in the asymmetric position of magnetic suspension when using split-type configurations. To solve the problem of asymmetry of captured magnetic flux, a configuration of HTS-rings with double split structure was proposed and calculated [157], which demonstrated more homogeneous distribution of magnetic field (Fig. 31) and a good temporary stability of the captured magnetic flux.

Coils and stacks of HTS-belts are calculated as an element of magnetic bearing for energy accumulators [141,142,158–165]. Both single coils [163], wafers [142], double wafers [164], and hybrid coils [162] can be used an HTS-coil. One more option of HTS-rings are loops of HTS-belts. The work [154] presents generalized model for the homogenization of HTS-loop and double wafer (Fig. 32), as well as the calculation of the vertical force based on the levitation gap for loop-type configuration (Fig. 33)

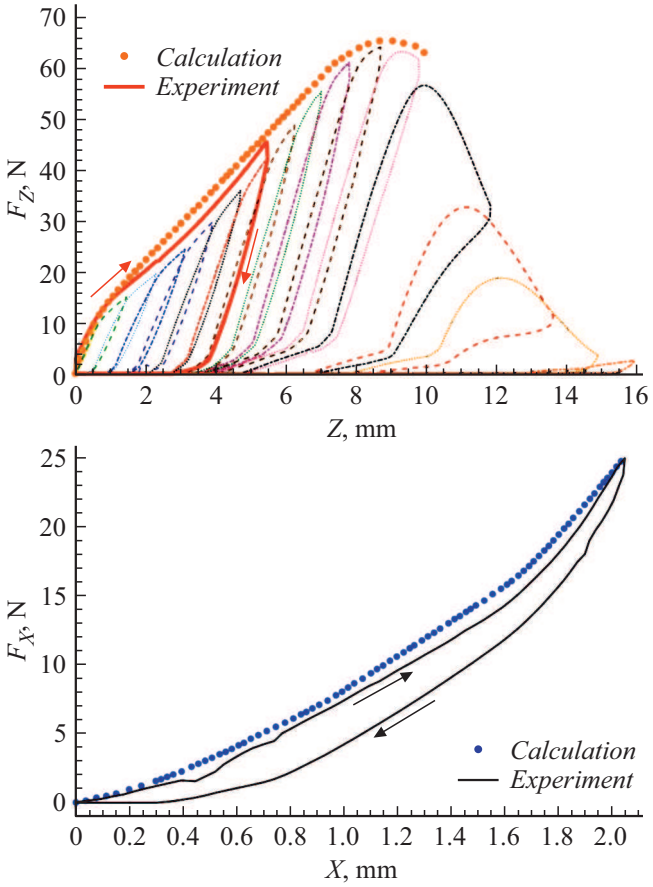

Figure 36. Loading curves for HTS-bearing in case of vertical (top) and lateral (bottom) shifts [136].

Either single permanent magnets or their assemblies in the form of co-oriented magnets [166,167], opposite-oriented magnets [148,168], as well as Halbach assembly [169,170] are the most frequently used in levitation systems. Comparison of the levitation force for HTS-belt stacks in the fields of different magnetic assemblies is given in the work [169]. It is shown that for using in transport systems, where it is required to maintain relatively high levitation gap, the use of opposite-oriented magnet assembly is more beneficial, meanwhile in the systems, where a priority parameter is the value of the levitation force, the use of Halbach magnet assembly is beneficial, because this provides a high interaction force, which, however, falls rapidly by height (Fig. 34).

3.6. Examples of calculation of real magnetic levitation systems

The work [171] provides calculations of loading curves and rotor oscillations for flywheel of a kinetic energy accumulator in the presence of angular shifts. In a series of works an analysis of electromagnetic characteristics of HTS-suspensions and bearings is performed by using (A−V)- and H-formulations in association with the model of equivalent electrical circuit [162,172]. As an example, we take a structure of a bearing based on open windings of HTS-belts from the work [148] (Fig. 35). Fig. 36 shows examples of loading curves of such HTS-bearing.

Transport position of HTS includes all possible magnetic suspensions and motors for a Maglev system, which is the conceptual model of a high-speed ground transport. Calculation models of HTS-motors are developed [173–175], as well as the models for calculation of dynamic motion resistance of suspension [176,177], calculation of the parameters of levitation system in case of vibrations [167,178], calculation of dynamic response and damping coefficient of HTS-belt stacks in the presence of external pulsed excitations [178], advantages and disadvantages of the use of three-dimensional HTS and HTS-belt stacks in levitation systems are shown [52,165].

The work [179] presents results of calculation of a linear superconducting motor based on HTS-belt stacks. The

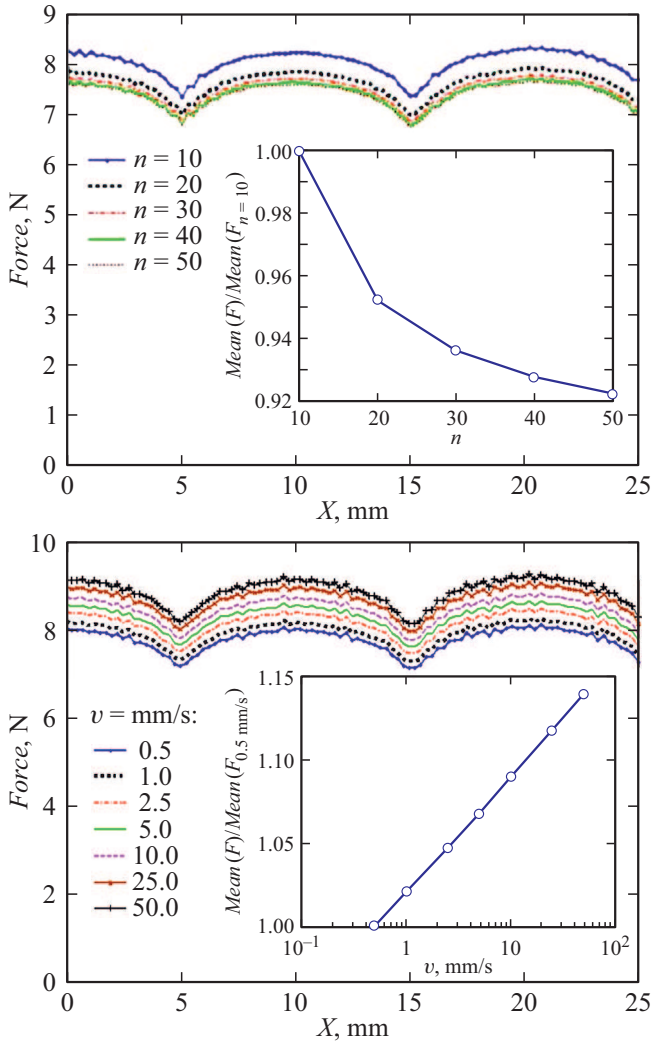

Figure 37. The levitation force of HTS-belt stack when moving above the magnetic assembly of opposite-oriented magnets for various values of the parameters of a power function of IU characteristic (top) and at various motion speeds (bottom) [164].

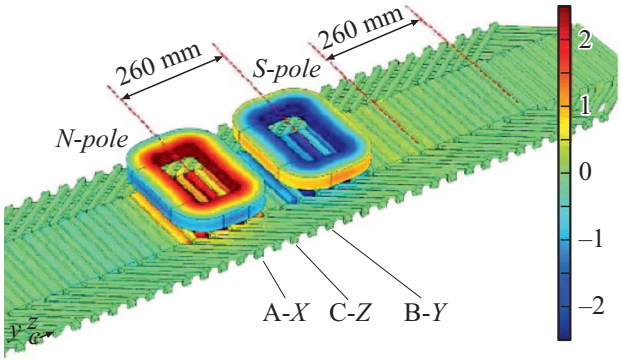

Figure 38. The concept of low-scale HTS-motor [165].

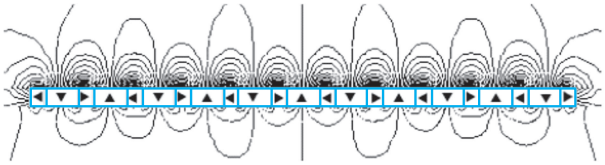

Flux lines of Halbach permanent magnet array

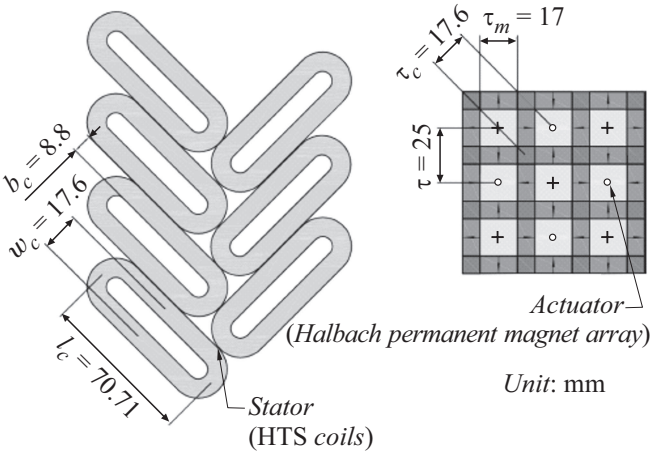

Platform of permanent magnet array and coil array

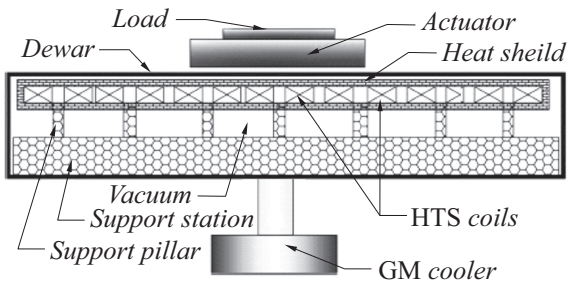

Structure diagram of SMLPM

Figure 39. Linear HTS-motor based on coils made of HTS-belts and Halbach array [154].

motor consists of a stator made of permanent opposite-oriented magnets and a stack of HTS-belts moving in the field of magnetic assembly. Calculation results are shown for various values „*n-value*“ of a power function of IU characteristic, as well as for different rotor motion speeds (Fig. 37).

Other option of a small-scale linear motor is given in [180]; it consists of HTS-belt wound coils placed into the field of similar magnetic assembly (Fig. 38). Use of such HTS-coils allows to minimize the total length of used belt for the provision of the required force. An improved model of a linear motor with the use of HTS-coils and Halbach magnetic assembly was presented in the work [170] (Fig. 39).

Modern cryogenic equipment enables easy achievement of the temperatures required for functioning of HTS-materials. Superconducting electrotechnical devices are promising for many areas, and, often have no alternatives. Today, there are examples of inclusion of superconducting devices into substations. Magnetic tomographs having a great significance for medicine, have one of the largest demand for superconductors. Such well known international projects, as the ITER and the Large Hadron Collider (LHC), solving global tasks and problems of physics and opening the next step for science, have become possible because of superconductors only. Today, the main part of powerful magnets of the LHC accelerator are either copper coils cooled by supercritical helium or superconductive coils made of low-temperature Nb_3Sn.

The use of HTS, in particular, HTS-belts, is planned to be tested at one of four main experiments in the LHC — ATLAS. Application of HTS in levitation systems opens perspectives for the development of the innovative modern high-speed transport and rotor systems. Design of such devices is always based on preliminary precise numerical analysis. The tools of mathematical modelling of physical processes occurring in the levitation systems of various scale allowed to calculate electrodynamic and thermophysical parameters of systems. The formulations described herein are based on the solution of Maxwell equations and are similar from this point of view. However, selection of relevant formulation for the solution of a certain physical task can reduce significantly the calculation time without considerable loss of accuracy. The H-formalism is considered as the most accurate and universal formulation at this moment. However, the solution of the task in terms of magnetic field components will require the availability of higher computation powers versus other existing approaches.

Conclusion

The presented review of literature data gives full enough description of physical principles of functioning and characteristics of various magnetic levitation systems both based on three-dimensional HTS-materials, and on new composite materials — superconductive belts assembled into stacks or used as windings. Application of HTS-belts instead

of conventional three-dimensional HTS has a series of advantages, regarding the following possibilities:

— creation of scalable magnetic levitation systems;

— easy creation of superconductive assemblies of virtually any forms and sizes, including complex three-dimensional structures;

— significant mechanical strength;

— improved thermal characteristics because of the presence of thermal conducting layers in the structure of composite, which is especially relevant in conditions of alternating magnetic loads:

— optimization of mass-dimension sizes of MLS.

To conclude, there are general recommendations for optimization of magnetic levitation devices based on HTS-belts:

1. Selection of HTS-belt

One of significant advantages of HTS-belts versus three-dimensional superconductors is a high density of critical current, however, this advantage is stolen by a low engineering (structural) density of current, since the filling coefficient for HTS is a bit higher than 1% at the substrate thickness of 100 μm. Based on it, in order to enhance the engineering density of current it is recommended to use the belts with thinner substrates in stacks — 40 or even 20 μm, which have already been produced by a series of companies.

Of course, it is required to select HTS-belts with the maximum possible critical current within the working range of magnetic fields up to 0.5 T (typical magnetic fields of the permanent magnet). The type of HTS, which is used in superconducting layers does not affect, if this HTS is of the REBCO family.

To create assemblies of HTS-belts one should use tinned belts, which allow to create dense HTS-blocks at low heating (up to 200°C).

2. Magnetic field parameters

The general recommendation on the use of permanent magnets is that a superconducting assembly must be within the region of the maximum gradient of magnetic field (and, as possible, in the region of the maximum field), which will lead to the maximum force of magnetic levitation. In a series of cases it is more preferable to use the Halbach array.

3. Optimization of mass-dimension sizes

Both the calculation and the experiment demonstrate the trend to saturation of the levitation force with the increase of the HTS-belt assembly thickness, associated with mutual shielding of belts in the assembly. This is why the use of thick assemblies is irrational. An optimum assembly thickness is considered to be 50−70 belts.

4. Selection of working temperature

Decrease of the working temperature, as results from calculations and experiment leads to the increase of the levitation force. However, at the level of fields of existing permanent magnets, decrease of the temperature below 65 K gives only a small benefit for the levitation force. Given that 65 K can be obtained by pumping the nitrogen vapors out, and lower temperatures require a complex cryogenic equipment, the use of low working temperatures is irrational.

5. Homogeneity of long magnetic assemblies

Long magnetic assemblies are used in a series of magnetic levitation applications, for example, magnetic levitation transport or magnetic levitation bearings. These assemblies should be made with the maximum possible homogeneity along the superconductor motion path, since the non-homogeneity of the magnetic field results in excessive magnetization of superconductor and occurrence of hysteresis losses. The last circumstance will inevitably result in the loss of magnetic levitation characteristics of the system.

To conclude, note that design of any magnetic levitation systems must be followed by the preliminary calculation of magnetic force characteristics for the selection of an optimum configuration of magnetic field and geometry of superconducting assembly.

Funding

The study was financially supported by the Russian Foundation for Basic Research as part of scientific project №20-18-50185 and scientific project № 20-3890144 (I.V. Anishchenko) under the „Aspirants“competition.

Conflict of interest

The authors declare that they have no conflict of interest.

References

[1] S. Earnshaw. Transactions of the Cambridge Philosophical Society, **7**, 97 (1848).

[2] M.V. Berry, A.K. Geim. Europ. J. Phys., **18** (4), 307 (1997). DOI: 10.1088/0143-0807/18/4/012

[3] A. Geim. Phys. Today, **51**, 36 (1998). DOI: 10.1063/1.882437

[4] A.K. Geim, M.D. Simon, M.I. Boamfa, L.O. Heflinger. Nature, **400**, 323 (1999). DOI: 10.1038/22444

[5] M.D. Simon, A.K. Geim. J. Appl. Phys., **87**, 6200 (2000). DOI: 10.1063/1.372654

[6] M.D. Ainslie, H. Fujishiro. Supercond. Scie.Technol., **28**, 053002 (2015). DOI: 10.1088/0953-2048/28/5/053002

[7] A. Ishihara, T. Akasaka, M. Tomita, K. Kishio. Supercond. Sci. Technol., **30**, 035006 (2017). DOI: 10.1088/1361-6668/30/3/035006

[8] J. Zou, M.D. Ainslie, H. Fujishiro, A.G. Bhagurkar, T. Naito, N. Hari Babu, J.F. Fagnard, P. Vanderbemden, A. Yamamoto. Supercond. Scie. Technol., **28**, 075009 (2015). DOI: 10.1088/0953-2048/28/7/075009

[9] H. Fujishiro, H. Mochizuki, M.D. Ainslie, T. Naito. Supercond. Sci. Technol., **29**, 084001 (2016). DOI: 10.1088/0953-2048/29/8/084001

[10] J.D. Weiss, A. Yamamoto, A.A. Polyanskii, R.B. Richardson, D.C. Larbalestier, E.E. Hellstrom. Supercond. Sci. Technol., **28**, 112001 (2015). DOI: 10.1088/0953-2048/28/11/112001

[11] K. Sawano, M. Morita, M. Tanaka, T. Sasaki, K. Kimura, S. Takebayashi, M. Kimura, K. Miyamoto. Jpn. J. Appl. Phys., **30**, L1157 (1991). DOI: 10.1143/jjap.30.l1157

[15] Y. Shi, J. H. Durrell, A.R. Dennis, K. Huang, D.K. Namburi, D. Zhou, D.A. Cardwell. Supercond. Sci. Technol., **30**, 015003 (2016). DOI: 10.1088/0953-2048/30/1/015003
[13] M. Ainslie, H. Fujishiro, T. Ujiie, J. Zou, A. Dennis, Y. Shi, D. Cardwell. Supercond. Sci. Technol., **27**, 065008 (2014). DOI: 10.1088/0953-2048/27/6/065008
[14] M. Tomita, M. Murakami. Supercond. Sci. Technol., **13**, 722 (2000). DOI: 10.1088/0953-2048/13/6/318
[15] S.B. Kim, J. Matsunaga, Y. Fujii, H. Onodera. IEEE Transactions on Appl. Superconduct., **23**, 4603204 (2013). DOI: 10.1109/TASC.2013.2242513
[16] S. Nariki, N. Sakai, M. Murakami, I. Hirabayashi. Supercond. Sci.Technol., **17**, S30 (2004). DOI: 10.1088/0953-2048/17/2/057
[17] M. Carrera, X. Granados, J. Amoros, R. Maynou, T. Puig, X. Obradors. IEEE Transactions on Appl. Superconduct., **19**, 3553 (2009). DOI: 10.1109/TASC.2009.2017764
[18] T. Ida, Z. Li, D. Zhou, M. Miki, Y. Zhang, M. Izumi. Supercond. Sci. Technol., **29**, 054005 (2016). DOI: 10.1088/0953-2048/29/5/054005
[19] C. Kim, J.-H. Joo, G.W. Hong, S.-C. Han, Y.H. Han, T. Sung, S.-J. Kim. Physica C Superconduct. Its Appl. PHYSICA C, **336**, 233 (2000). DOI: 10.1016/S0921-4534(00)00292-6
[20] A. Murakami, H. Teshima, M. Morita, T. Kudo, A. Iwamoto. J. Physics: Conf. Series, **507**, 012034 (2014). DOI: 10.1088/1742-6596/507/1/012034
[21] S. Jin, T.H. Tiefel, R.C. Sherwood, R.B. van Dover, M.E. Davis, G.W. Kammlott, R.A. Fastnacht. Phys. Rev. B, **37**, 7850 (1988). DOi: 10.1103/PhysRevB.37.7850
[22] K. Salama, V. Selvamanickam, L. Gao, K. Sun. Appl. Phys. Lett., **54**, 2352 (1989). DOI: 10.1063/1.101525
[23] M. Murakami, M. Morita, K. Doi, K. Miyamoto. Jpn J. Appl. Phys., **28**, 1189 (1989). DOI: 10.1143/jjap.28.1189
[24] H. Fujimoto, M. Murakami, S. Gotoh, N. Koshizuka, T. Oyama, Y. Shiohara, S. Tanaka, in Advances in Superconductivity II, T. Ishiguro, K. Kajimura, eds. (Springer Japan, Tokyo, 1990), p. 285–288.
[25] Z. Lian, Z. Pingxiang, J. Ping, W. Keguang, W. Jingrong, W. Xiaozu. Supercondu. Sci. Technol., **3**, 490 (1990). DOI: 10.1088/0953-2048/3/10/002
[26] D. Shi, S. Sengupta, J.S. Luo, C. Varanasi, P.J. McGinn. Physica C: Superconduct. Applicat., **213**, 179 (1993). DOI: 10.1016/0921-4534(93)90774-K
[27] P. de Rango, M. Lees, P. Lejay, A. Sulpice, R. Tournier, M. Ingold, P. Germi, M. Pernet. Nature, **349**, 770 (1991). DOI: 10.1038/349770a0
[28] Y. Yamada, Y. Shiohara. Physica C: Superconduct., **217**, 182 (1993). DOI: 10.1016/0921-4534(93)90810-D
[29] H. Walter, M.P. Delamare, B. Bringmann, A. Leenders, H.C. Freyhardt. J. Mater. Res., **15**, 1231 (2000). DOI: 10.1557/JMR.2000.0175
[30] G. Fuchs, P. Schätzle, G. Krabbes, S. Gruß, P. Verges, K.H. Müller, J. Fink, L. Schultz. Appl. Phys. Lett., **76**, 2107 (2000). DOI: 10.1063/1.126278
[31] J.V. Yakhmi, in *An interdisciplinary approach* (IOP Publishing, 2021). DOI: 10.1088/978-0-7503-2256-0
[32] N. Ayai, M. Kikuchi, K. Yamazaki, S. Kobayashi, S. Yamade, E. Ueno, N. J. Fujikami, T. Kato, K. Hayashi, K. Sato, R. Hata, J. Iihara, K.J. Yamaguchi, J. Shimoyama. IEEE Transactions Appl. Superconduct., **17**, 3075 (2007). DOI: 10.1109/TASC.2007.897947
[33] D.A. Cardwell, D.C. Larbalestier. *Handbook of Superconducting Materials, 2nd Edition (3-Volume Set).* (Taylor & Francis, 2017)
[34] S.R. Foltyn, L. Civale, J.L. MacManus-Driscoll, Q.X. Jia, B. Maiorov, H. Wang, M. Maley. Nature Materia., **6**, 631 (2007). DOI: 10.1038/nmat1989
[35] P.N. Arendt. *IBAD Template Films for HTS Coated Conductors,* A. Goyal, Ed. (Springer US, Boston, MA, 2005), DOI: 10.1007/0-387-25839-6_1
[36] J.L. MacManus-Driscoll, S.C. Wimbush. Nature Rev. Mater., **6**, 587 (2021). DOI: 10.1038/s41578-021-00290-3
[37] A. Sundaram, Y. Zhang, A. Knoll, D. Abraimov, P. Brownsey, M. Kasahara, G. Carota, R. Nakasaki, J. Cameron, G. Schwab, L. Hope, R. Schmidt, H. Kuraseko, T. Fukushima, D. Hazelton. Supercond. Sci. Technol., **29**, 104007 (2016). DOI: 10.1088/0953-2048/29/10/104007
[38] Electronic source. Available at: https://www.theva.com/products/
[39] Electronic source. Available at: http://www.super- power-inc.com/content/2g-hts-wire
[40] K. Tsuchiya, A. Kikuchi, A. Terashima, K. Norimoto, M. Uchida, M. Tawada, M. Masuzawa, N. Ohuchi, X. Wang, T. Takao, S. Fujita. Cryogenics, **85**, 1 (2017). DOI: 10.1016/j.cryogenics.2017.05.002
[41] A. Patel, V. Kalitka, S. Hopkins, A. Baskys, A. Figini Albisetti, G. Giunchi, A. Molodyk, B.A. Glowacki. IEEE Transactions Appl. Superconducti., **26**, 1 (2016). DOI: 10.1109/TASC.2016.2524468
[42] M. Tomita, M. Murakami. Nature, **421**, 517 (2003). DOI: 10.1038/nature01350
[43] J. Durrell, A. Dennis, J. Jaroszynski, M. Ainslie, K. Palmer, Y. Shi, A. Campbell, J. Hull, M. Strasik, E. Hellstrom, D. Cardwell. Supercond. Sci. Technol,, **27**, 082001 (2014). DOI: 10.1088/0953-2048/27/8/082001
[44] Electronic source. Available at: www.superpower-inc.com/content/wire-specification
[45] A. Patel, K. Filar, V. Nizhankovskii, S. Hopkins, B.A. Glowacki. Appl. Phys. Lett., **102**, 102601 (2013). DOI: 10.1063/1.4795016
[46] A. Baskys, A. Patel, S. Hopkins, V. Kalitka, A. Molodyk, B.A. Glowacki. IEEE Transactions Appl. Superconduct., **25**, 1 (2015). DOI: 10.1109/TASC.2014.2360871
[47] A. Patel, A. Baskys, T. Mitchell-Williams, A. McCaul, W. Coniglio, B.A. Glowacki. Supercond. Sci.Technol., **31** (2017). DOI: 10.1088/1361-6668/aad34c
[48] F. Sass, G. Sotelo, R. Jr, F. Sirois. Supercond. Sci. Technol., **28**, 125012 (2015). DOI: 10.1088/0953-2048/28/12/125012
[49] D. Brown, B.-M. Ma, Z. Chen. J. Magnetism and Magnetic Mater., **248**, 432 (2002). DOI: 10.1016/S0304-8853(02)00334-7
[50] M. Sagawa, S. Hirosawa, H. Yamamoto, S. Fujimura, Y. Matsuura. Jpn. J. Appl. Phys., **26**, 785 (1987). DOI: 10.1143/JJAP.26.785
[51] B.M. Ma, J.W. Herchenroeder, B. Smith, M. Suda, D. Brown, Z. Chen. J. Magnetism and Magnetic Mater., **239**, 418 (2002). DOI: 10.1016/S0304-8853(01)00609-6
[52] P. Bernstein, J. Noudem. Supercond. Sci.Technol., **33**, 033001 (2020). DOi: 10.1088/1361-6668/ab63bd
[53] I. Rudnev, M. Osipov, S. Pokrovskii, A. Podlivaev. Mater. Res. Express, **6**, 036001 (2018). DOI: 10.1088/2053-1591/aaf7ae

[54] M. Osipov, A. Starikovskii, I. Anischenko, S. Pokrovskii, D. Abin, I. Rudnev. Supercond. Sci.Technol., **34** (4), 045003 (2021). DOI: 10.1088/1361-6668/abe18e
[55] J. Wang, S. Wang, C. Deng, J. Zheng, H. Song, Q. He, Y. Zeng, Z. Deng, J. Li, G. Ma, H. Jing, Y. Huang, J. Zhang, Y. Lu, L. Liu, L. Wang, J. Zhang, L. Zhang, M. Liu, Y. Qin, Y. Zhang. IEEE Transactions Appl. Superconduct., **17**, 2091 (2007). DOI: 10.1109/TASC.2007.898367
[56] D.H.N. Dias, G.G. Sotelo, R. de Andrade. IEEE Transactions on Appl. Superconduct., **21**, 1533 (2011). DOI: 10.1109/TASC.2010.2090635
[57] W. Yang, X. Chao, X. Bian, P. Liu, Y. Feng, P. Zhang, L. Zhou. Supercond. Sci. Technol., **16**, 789 (2003). DOI: 10.1088/0953-2048/16/7/308
[58] T. Suzuki, E. Ito, T. Sakai, S. Koga, M. Murakami, K. Nagashima, Y. Miyazaki, H. Seino, N. Sakai, I. Hirabayashi, K. Sawa. IEEE Transactions Appl. Superconduct., **17**, 3020 (2007). DOI: 10.1109/TASC.2007.899403
[59] P. Bernstein, L. Colson, L. Dupont, J. Noudem. Supercond. Sci. Technol., **30**, 065007 (2017). DOI: 10.1088/1361-6668/aa69ec
[60] A. Sanchez, N. Del-Valle, C. Navau, D.-X. Chen. J. Appl. Phys., **105**, 023906 (2009). DOI: 10.1063/1.3054922
[61] M.J. Qin, G. Li, H.K. Liu, S.X. Dou, E.H. Brandt. Phys. Rev. B, **66**, 024516 (2002). DOI: 10.1103/PhysRevB.66.024516
[62] H. Jing, J. Wang, S. Wang, L. Wang, L. Liu, J. Zheng, Z. Deng, G. Ma, Y. Zhang, J. Li. Physica C: Superconduct. and its Applications, **463**–**465**, 426 (2007). DOI: 10.1016/j.physc.2007.05.030
[63] N. Del-Valle, A. Sanchez, C. Navau, D.-X. Chen. J. Low Temperature Phys., **162**, 62 (2011). DOI: 10.1007/s10909-010-0225-0
[64] G.G. Sotelo, D.H.N. Dias, R. de Andrade, R.M. Stephan. IEEE Transactions on Appl. Superconduct., **21**, 1464 (2011). DOI: 10.1109/TASC.2010.2086034
[65] H. Liao, J. Zheng, L. Jin, H. Huang, Z. Deng, Y. Shi, D. Zhou, D. Cardwell. Supercond. Sci. Technol., **31** (3), (2018). DOI: 10.17863/CAM.21602
[66] W. Liu, J.S. Wang, G. Ma, J. Zheng, X.G. Tuo, L.L. Li, C.-Q. Ye, X.-L. Liao, S. Wang. Physica C: Superconduct., **474**, 5 (2012). DOI: 10.1016/j.physc.2011.12.005
[67] T. Che, Y.F. Gou, J. Zheng, R.X. Sun, D.B. He, Z.G. Deng. J. Superconduct. Novel Magnetism, **27**, 2211 (2014). DOI: 10.1007/s10948-014-2596-y
[68] D.H.N. Dias, G.G. Sotelo, F. Sass, E.S. Motta, R. de Andrade Jr, R.M. Stephan. Phys. Proced., **36**, 1049 (2012). DOI: 10.1016/j.phpro.2012.06.104
[69] W. Yang, Y. Liu, Z. Wen, X. Chen, Y. Duan. Supercond. Sci. Technol., **21**, 015014 (2007). DOI: 10.1088/0953-2048/21/01/015014
[70] F. Sass, D.H.N. Dias, G.G. Sotelo, R. de Andrade Jr. Physi. Proced., **36**, 1008 (2012). DOI: 10.1016/j.phpro.2012.06.097
[71] F. Sass, D.H.N. Dias, G.G. Sotelo, R. de Andrade. IEEE Transactions on Appl. Superconduct., **23**, 3600905 (2013). DOI: 10.1109/TASC.2012.2234172
[72] S.V. Pokrovskiy, N. Mineev, A. Sotnikova, Y. Ermolaev, I. Rudnev. J. Physics: Conf. Series, **507**, 022025 (2014). DOI: 10.1088/1742-6596/507/2/022025
[73] I. Rudnev, D. Abin, M. Osipov, S.V. Pokrovskiy, Y. Ermolaev, N. Mineev. Phys. Proced., **65**, 141 (2015). DOI: 10.1016/j.phpro.2015.05.086
[74] M.A. Osipov, D.A. Abin, S.V. Pokrovskiy, N.A. Mineev, I.A. Rudnev. Progress in Superconduct. Cryogenics, **17**, 21 (2015).
[75] D. Abin, M. Osipov, S.V. Pokrovskiy, I. Rudnev. IEEE Transactions on Appl. Superconduct., **26**, 1 (2016). DOI: 10.1109/TASC.2016.2525924
[76] S.V. Pokrovskiy, M. Osipov, D. Abin, I. Rudnev. IEEE Transactions on Appl. Superconduct., **26**, 1 (2016). DOI: 10.1109/TASC.2016.2533573
[77] M. Osipov, A. Starikovskii, D. Abin, I. Rudnev. Supercond. Sci. Technolo., **32**, 054003 (2019). DOI: 10.1088/1361-6668/ab06e6
[78] K. Liu, W. Yang, G. Ma, L. Quéval, T. Gong, C. Ye, X. Li, Z. Luo. Supercond. Sci. Technol., **31**, 015013 (2017). DOI: 10.1088/1361-6668/aa987b
[79] I. Anischenko, S. Pokrovskii, I. Rudnev. J. Physics: Conf. Series, **1238**, 012020 (2019). DOI: 10.1088/1742-6596/1238/1/012020
[80] J. Ma, J. Geng, W.K. Chan, J. Schwartz, T. Coombs. Supercond. Sci. Technol., **33**, 045007 (2020). DOI: 10.1088/1361-6668/ab6fe9
[81] J. Ma, T. Coombs, J. Geng, W. Chan, J. Gawith, C. Li, B. Shen, Y. Öztürk, J. Yang, J. Hu. IEEE Transactions on Appl. Superconduct., **30** (4), 1 (2020). DOI: 10.1109/TASC.2020.2977004
[82] S. Gyimóthy, A. Kenderes, S. Bilicz, J. Pávó, Z. Badics, in 2019 22nd Intern. Conf. on the DOI: 10.1109/COMPUMAG45669.2019.9032824
[83] V. Zermeno, A. Abrahamsen, N. Mijatovic, B. Jensen, M. Sørensen. J. Appl. Phys., **114**, 173901 (2013). DOI: 10.1063/1.4827375
[84] S. Zou, V. Zermeño, F. Grilli. arXiv preprint arXiv: 1511.00516 (2015).
[85] S. Zou, V.M.R. Zermeño, F. Grilli. IEEE Transactions on Appl. Superconduct., **26**, 1 (2016). DOI: 10.1109/TASC.2016.2535379
[86] I.V. Anischenko, S.V. Pokrovskii, I.A. Rudnev. J. Physics: Conf. Series, **1238**, 012020 (2019). DOI: 10.1088/1742-6596/1238/1/012020
[87] A. Podlivaev, I. Rudnev, N. Shabanova. Bull. Lebedev Physi. Institute, **41**, 351 (2015). DOI: 10.3103/S1068335614120033
[88] M.J. Wolf, R. Heller, W.H. Fietz, K.-P. Weiss. Cryogenics, **104**, 102980 (2019). DOI: 10.1016/j.cryogenics.2019.102980
[89] X. Zhang, Z. Zhong, J. Geng, B. Shen, J. Ma, C. Li, H. Zhang, Q. Dong, T. Coombs. J. Superconduct. Novel Magnetism, **31**, 3847 (2018). DOI: 10.1007/s10948-018-4678-8
[90] I.V. Anischenko, S.V. Pokrovskii, I.A. Rudnev. J. Physics: Conf. Series, **1389**, 012064 (2019). DOI: 10.1088/1742-6596/1389/1/012064
[91] E.H. Brandt. Phys. Rev. B, **54**, 4246 (1996). DOI: 10.1103/PhysRevB.54.4246
[92] L. Prigozhin. IEEE Transactions on Appl. Superconduct., **7**, 3866 (1997). DOI: 10.1109/77.659440
[93] K. Berger, J. Lévêque, D. Netter, B. Douine, A. Rezzoug. IEEE Transactions on Appl. Superconduct., **15** (2), 1508 (2005). DOI: 10.1109/TASC.2005.849149
[94] G.J. Barnes, D. Dew-Hughes, M.D. McCulloch. Supercond. Sci.Technol., **13**, 229 (2000). DOI: 10.1088/0953-2048/13/2/319

[95] K.K. Pradhan, S. Chakraverty. *Computational Structural Mechanics: Static and Dynamic Behaviors* (Academic Press, London, 2019), p. 25–28. DOI: 1016/B978-0-12-815492-2.00010-1
[96] J. Das, R.N. Ray, in 2017 8th Annual Industrial Automation and Electromechanical Engineer. Conf. (IEMECON). (2017), p. 96–100. DOI: 10.1109/IEMECON.2017.8079569
[97] B. Shen, C. Li, J. Geng, X. Zhang, J. Gawith, J. Ma, Y. Liu, F. Grilli, T. Coombs. Superconduc. Sci. Technol., **31** (7), 075005 (2018). DOI: 10.1088/1361-6668/aac294
[98] R. Kulkarni, K. Prasad, T.T. Lie, R. Badcock, C. Bumby, H.-J. Sung. Energies, **10**, 1344 (2017). DOI: 10.3390/en10091344
[99] K. Zhang, M. Ainslie, M. Calvi, S. Hellmann, R. Kinjo, T. Schmidt. Supercondu. Scien. Technol., **33**, 114007 (2020). DOI: 10.1088/1361-6668/abb78a
[100] C. Lorin, D. Netter, P.J. Masson. IEEE Transactions on Appl. Superconduct., **25**, 1 (2015). DOI: 10.1109/TASC.2014.2341255
[101] M.D. Ainslie, T.J. Flack, Z.Hong, T.A. Coombs. The International J. Computation and Mathematics in Electrical and Electronic Engineering, **30**, 762 (2011). DOI: 10.1108/03321641111101195
[102] M. Zhang, T.A. Coombs. Supercond. Sci. Technol., **25**, 015009 (2011). DOI: 10.1088/0953-2048/25/1/015009
[103] V.M.R. Zermeno, F. Grilli, F. Sirois. Supercond. Sci. Technol., **26**, 052001 (2013). DOI: 10.1088/0953-2048/26/5/052001
[104] V.M.R. Zermeño, F. Grilli. Supercond. Sci. Technol., **27**, 044025 (2014). DOI: 10.1088/0953-2048/27/4/044025
[105] W. Ta, Y. Li, Y. Gao. AIP Advances, **4**, 087131 (2014). DOI: 10.1063/1.4893770
[106] R. Brambilla, F. Grilli, L. Martini. Supercond. Sci. Technol., **20**, 16 (2006). DOI: 10.1088/0953-2048/20/1/004
[107] A.M. Campbell. Supercond. Sci. Technol., **22**, 034005 (2009). DOI: 10.1088/0953-2048/22/3/034005
[108] N. Amemiya, S.-ichi Murasawa, N. Banno, K. Miyamoto. Physica C: Superconduct., **310**, 16 (1998). DOI: 10.1016/S0921-4534(98)00427-4
[109] G. Meunier, Y. Floch, C. Guérin. Magnetics, IEEE Transactions on Appl. Superconduct., **39**, 1729 (2003). DOI: 10.1109/TMAG.2003.810200
[110] S. Mykola, G. Fedor. Supercond. Sci. Technol., **32**, 115001 (2019). DOI: 10.1088/1361-6668/ab3a85
[111] H. Zhang, M. Zhang, W. Yuan. Supercond. Sci. Technol., **30**, 024005 (2016). DOI: 10.1088/1361-6668/30/2/024005
[112] F. Grilli, R. Brambilla, L. Martini. IEEE Transactions on Appl. Superconduct., **17**, 3155 (2007). DOI: 10.1109/TASC.2007.902144
[113] F. Grilli, R. Brambilla, F. Sirois, A. Stenvall, S. Memiaghe. Cryogenics, **53**, 142 (2013). DOI: 10.1016/j.cryogenics.2012.03.007
[114] C. Hofmann, G. Ries. Supercond. Sci. Technol., **14**, 34 (2000). DOI: 10.1088/0953-2048/14/1/306
[115] D.H.N. Dias, E.S. Motta, G.G. Sotelo, R. de Andrade, R.M. Stephan, L. Kuehn, O. de Haas, L. Schultz. IEEE Transactions on Appl. Superconduct., **19**, 2120 (2009). DOI: 10.1109/TASC.2009.2019203
[116] D. Dias, E. Motta, G. Sotelo, R. de Andrade Jr. Supercond. Sci. Technol., **23**, 075013 (2010). DOI: 10.1088/0953-2048/23/7/075013
[117] G. Ma. IEEE Transactions on Appl. Superconduct., **23**, 3601609 (2013). DOI: 10.1109/TASC.2013.2259488
[118] G.-T. Ma, H. Liu, X.-T. Li, H. Zhang, Y.-Y. Xu. J. Appl. Phys., **115**, 083908 (2014). DOI: 10.1063/1.4867160
[119] C. Ye, G. Ma, J. Wang. IEEE Transactions on Appl. Superconduct., **26**, 1 (2016). DOI: 10.1109/TASC.2016.2615120
[120] T. Sugiura, H. Hashizume, K. Miya. Intern. J. Appl. Electromagnetics in Materials, **2** (3), 183 (1991).
[121] N. Takeda, M. Uesaka, K. Miya. Cryogenics, **34**, 745 (1994). DOI: 10.1016/0011-2275(94)90161-9
[122] C. Yon-Do, K. Youn-Hyun, L. Ju, H. Jung-Pyo, L. Jong-Woo. IEEE Transactions on Appl. Superconducti., **11**, 2000 (2001). DOI: 10.1109/77.920246
[123] D. Ruiz-Alonso, T.A. Coombs, A.M. Campbell. IEEE Transactions on Appl. Superconduct., **14**, 2053 (2004). DOI: 10.1109/TASC.2004.838316
[124] G. Sotelo, R. de Andrade, A. Ferreira. IEEE Transactions on Appl. Superconduct., **19**, 2083 (2009). DOI: 10.1109/TASC.2009.2019555
[125] H. Ueda, S. Azumaya, S. Tsuchiya, A. Ishiyama. IEEE Transactions on Appl. Superconduct., **16**, 1092 (2006). DOI: 10.1109/TASC.2006.871280
[126] A.O. Hauser. IEEE Transactions on Magnetics, **33**, 1572 (1997). DOI: 10.1109/20.582566
[127] J. Zhang, Y. Zeng, J. Cheng, X. Tang. IEEE Transactions on Appl. Superconduct., **18**, 1681 (2008). DOI: 10.1109/TASC.2008.2000900
[128] X. Zheng, Y. Yang. IEEE Transactions on Appl. Superconduct., **17**, 3862 (2007). DOI: 10.1109/TASC.2007.910150
[129] X. Gou, X. Zheng, Y. Zhou. IEEE Transactions on Appl. Superconduct., **17**, 3795 (2007). DOI: 10.1109/TASC.2007.902104
[130] Y. Yoshida, M. Uesaka, K. Miya. IEEE Transactions on Magnetics, **30**, 3503 (1994). DOI: 10.1109/20.312694
[131] M. Tsuchimoto, T. Honma. IEEE Transactions on Appl. Superconduct., **4**, 211 (1994). DOI: 10.1109/77.334961
[132] M. Tsuda, H. Lee, Y. Iwasa. Cryogenics, **38**, 743 (1998). DOI: 10.1016/S0011-2275(98)00049-6
[133] M. Tsuda, H. Lee, S. Noguchi, Y. Iwasa. Cryogenics, **39**, 893 (1999). DOI: 10.1016/S0011-2275(99)00125-3
[134] H. Ueda, A. Ishiyama. Supercond. Sci. Technol., **17**, S170 (2004). DOI: 10.1088/0953-2048/17/5/016
[135] G. Ma, J. Wang, S. Wang. IEEE Transactions on Appl. Superconduct., **20**, 2219 (2010). DOI: 10.1109/TASC.2010.2044795
[136] G. Ma, J. Wang, S. Wang. IEEE Transactions on Appl. Superconduct., **20**, 2228 (2010). DOI: 10.1109/TASC.2010.2044936
[137] S. Pratap, C. S. Hearn. IEEE Transactions on Appl.Superconduct. **25**, 1 (2015). DOI: 10.1109/TASC.2015.2470670
[138] Y. Lu, Y. Qin. Intern. J. Modern Phys. B, **29**, 1542038 (2015). DOI: 10.1142/S0217979215420382
[139] Y. Lu, J. Wang, S. Wang, J. Zheng. J. Superconduct. Novel Magnetism, **21**, 467 (2008). DOI: 10.1007/s10948-008-0386-0
[140] L. Quéval, G.G. Sotelo, Y. Kharmiz, D.H.N. Dias, F. Sass, V.M.R. Zermeño, R. Gottkehaskamp. IEEE Transactions on Appl. Superconduct., **26**, 1 (2016). DOI: 10.1109/TASC.2016.2528989

[141] L. Quéval, K. Liu, W. Yang, V.M.R. Zermeño, G.Ma. Supercond. Sci. Technol., **31**, 084001 (2018). DOI: 10.1088/1361-6668/aac55d
[142] A. Patel, S.C. Hopkins, A. Baskys, V. Kalitka, A. Molodyk, B.A. Glowacki. Supercond. Sci. Technol., **28**, 115007 (2015). DOI: 10.1088/0953-2048/28/11/115007
[143] E. Berrospe-Juarez, V.M.R. Zermeño, F. Trillaud, F. Grilli. Supercond. Sci. Technol., **32**, 065003 (2019). DOI: 10.1088/1361-6668/ab0d66
[144] F. Liang, S. Venuturumilli, H. Zhang, M. Zhang, J. Kvitkovic, S. Pamidi, Y. Wang, W. Yuan. J. Appl. Phys., **122**, 043903 (2017). DOI: 10.1063/1.4995802
[145] H. Zhang, K. Kails, P. Machura, M. Mueller. IEEE Transactions on Appl. Superconduct., **31** (5), 1 (2021). DOI: 10.1109/TASC.2021.3061021
[146] F. Sass, D.H.N. Dias, G.G. Sotelo, R. de Andrade Jr. Supercond. Sci. Technol., **31**, 025006 (2018). DOI: 10.1088/1361-6668/aa9dc1
[147] V.M. Rodriguez-Zermeno, N. Mijatovic, C. Traeholt, T. Zirngibl, E. Seiler, A.B. Abrahamsen, N.F. Pedersen, M.P. Sorensen. IEEE Transactions on Appl. Superconduct., **21**, 3273 (2011). DOI: 10.1109/TASC.2010.2091388
[148] M. Osipov, I. Anishenko, A. Starikovskii, D. Abin, S. Pokrovskii, A. Podlivaev, I. Rudnev. Supercond. Sci. Technol., **34**, 035033 (2021). DOI: 10.1088/1361-6668/abda5a
[149] J.R. Clem, J.H. Claassen, Y. Mawatari. Supercond. Sci. Technol., **20**, 1130 (2007). DOI: 10.1088/0953-2048/20/12/008
[150] W. Yuan, A.M. Campbell, T.A. Coombs. Supercond. Sci. Technol., **22**, 075028 (2009). DOI: 10.1088/0953-2048/22/7/075028
[151] L. Prigozhin, V. Sokolovsky. Supercond. Sci. Technol., **24**, 075012 (2011). DOI: 10.1088/0953-2048/24/7/075012
[152] I.V. Anischenko, S.V. Pokrovskii, I.A. Rudnev. J. Physics: Conf. Series, **945**, 012015 (2018). DOI: 10.1088/1742-6596/945/1/012015
[153] A. Patel, S. Hahn, J.P. Voccio, A. Baskys, S. Hopkins, B.A. Glowacki. Supercond. Sci. Technol., **30**, 024007 (2017). DOI: 10.1088/1361-6668/30/2/024007
[154] F. Martins, F. Sass, R. de Andrade Jr. Supercond. Sci. Technol., **32**, 044002 (2019). DOI: 10.1088/1361-6668/aafd08
[155] J. Sheng, M. Zhang, Y. Wang, X. Li, J. Patel, W. Yuan. Supercond. Sci. Technol., **30**, 094002 (2017). DOI: 10.1088/1361-6668/aa7a51
[156] I. Anishchenko, S. Pokrovskii, I. Rudnev. Bull. Lebedev Phys. Institute, **45**, 373 (2018). DOI: 10.3103/S1068335618120011
[157] D. Qiu, W. Wu, Y. Pan, S. Xu, Z.M. Zhang, Z. L. Li, Z.Y. Li, Y. Wang, L. Wang, Y. Zhao, Z.W. Zhang, P. Yang, Z. Hong, Z. Jin. IEEE Transactions on Appl. Superconduct., **27**, 1 (2017). DOI: 10.1109/TASC.2017.2652538
[158] Y. Xu, L. Ren, Z. Zhang, Y. Tang, J. Shi, C. Xu, J. Li, D. Pu, Z. Wang, H. Liu, L. Chen. Energy, **143**, 372 (2018). DOI: 10.1016/j.energy.2017.10.087
[159] Z. Wang, Y. Tang, L. Ren, J. Li, Y. Xu, Y. Liao, X. Deng. IEEE Transactions on Appl. Superconduct., **27** (4), 1 (2016). DOI: 10.1109/TASC.2016.2646480
[160] S.S. Peng, J. Zheng, W.Y. Li, Y.J. Dai. IOP Conf. Series: Earth and Environmental Sci., **233**, 022018 (2019). DOI: 10.1088/1755-1315/233/2/022018
[161] A. Kumar, J.V.M.L. Jeyan, A. Agarwal. Mater. Today: Proceed., **21**, 1755 (2020). DOI: 10.1016/j.matpr.2020.01.228
[162] J. Zhu, M. Qiu, B. Wei, H. Zhang, X. Lai, W. Yuan. Energy, **51**, 184 (2013). DOI: 10.1016/j.energy.2012.09.044
[163] N. Amaro, J.M. Pina, J. Martins, J.M. Ceballos, in *Technological Innovation for the Internet of Things,* L.M. Camarinha-Matos, S. Tomic, P. Graça, Eds. (Springer Berlin Heidelberg, 2013), p. 449–456.
[164] R. Gupta, M. Anerella, P. Joshi, J. Higgins, S. Lalitha, W. Sampson, J. Schmalzle, P. Wanderer. IEEE Transactions on Appl. Superconduct., **26**, 1 (2016). DOI: 10.1109/TASC.2016.2517404
[165] E. Kurbatova, E. Kushchenko, P. Kurbatov, in *21st International Symposium on Electrical Apparatus & Technologies (SIELA).* (2020), p. 1–4. DOI: 10.1109/SIELA49118.2020.9167096
[166] I.S.P. Peixoto, F.F. da Silva, J.F.P. Fernandes, P.J. da C. Branco. IEEE Transactions on Appl. Superconduct., **31**, 1 (2021). DOI: 10.1109/TASC.2021.3057570
[167] L. Chen, Z. Deng, B. Deng, J. Zheng. J. Superconduct. Novel Magnetism, (2021). DOI: 10.1007/s10948-020-05780-z
[168] J. Liang, J. Jin, R. Zhang, G. Bai, in *IEEE International Conference on Applied Superconductivity and Electromagnetic Devices (ASEMD).* (2020), p. 1–2. DOI: 10.1109/ASEMD49065.2020.9276246
[169] I. Anischenko, S. Pokrovskii, I. Rudnev, M. Osipov. Superconduct. Sci. Technol., **32**, 9 (2019). DOI: 101088/1361-6668/ab2bbe
[170] Y. Zhang, K. Ding, S. Du. IEEE Transactions on Appl. Superconduct., **31**, 1 (2021). DOI: 10.1109/TASC.2021.3062781
[171] G. Homrich, A.F.F. Filho, D.G. Dorrell, B. Dias, in *46th Annual Conference of the IEEE Industrial Electronics Society.* (2020), p. 937–942. DOI: 10.1109/IECON43393.2020.9254589
[172] A.R. Kim, J.G. Kim, S. Kim, M. Park, I.K. Yu, K.C. Seong, K. Watanabe. Physica C: Superconduct. Applicat., **471**, 1404 (2011). DOI: 10.1016/j.physc.2011.05.204
[173] G. Li, X. Wang, P. Cui, J. Li. Cluster Computing, **22**, 2709 (2019). DOI: 10.1007/s10586- 017-1434-y
[174] S.Y. Choi, C.Y. Lee, J.M. Jo, J.H. Choe, Y.J. Oh, K.S. Lee, J.Y. Lim. Energies, **12** (24), 4611 (2019). DOI: 10.3390/en12244611
[175] F.J.M. Dias, A. Polasek, R. de Andrade, E. Rodriguez, F. Costa, G.G. Sotelo, in *Simposio Brasileiro de Sistemas Eletricos (SBSE).* (2018), p. 1–5. DOI: 10.1109/SBSE.2018.8395656
[176] J. Wang, F. Cai, J. Jiang, L. Zhao, Y. Zhao, Y. Zhang. Physica C: Superconduct. Applicat., **581**, 1353809 (2021). DOI: 10.1016/j.physc.2020.1353809
[177] Z. Zhao, S. Xu, K. Liu, W. Yang, J. Li, G. Ma. J. Superconduct. Novel Magnetism, **34**, 75 (2021). DOI: 10.1007/s10948-020-05684-y
[178] K. Liu, G. Ma, C. Ye, W. Yang, G. Li, Z. Luo, Y. Cai. IEEE Transactions on Appl. Superconduct., **28**, 1 (2018). DOI: 10.1109/TASC.2018.2797098

[179] G.G. Sotelo, F. Sass, M. Carrera, J. Lopez-Lopez, X. Granados. IEEE Transactions on Industrial Electron., **65**, 7477 (2018). DOI: 10.1109/TIE.2018.2793252
[180] F. Dong, Z. Huang, D. Qiu, L. Hao, W. Wu, Z. Jin. in *2018 IEEE International Conference on Applied Superconductivity and Electromagnetic Devices (ASEMD)* (2018), p. 1–2. DOI: 10.1109/ASEMD.2018.8558945